

Stochastic Modeling and Simulation of Frequency-Correlated Wideband Fading Channels

Cheng-Xiang Wang, *Member, IEEE*, Matthias Pätzold, *Senior Member, IEEE*, and Qi Yao

Abstract—For the simulation of practical frequency-diversity wireless communication systems, such as frequency-hopping systems, multicarrier code-division multiple-access systems, and orthogonal frequency-division multiplexing systems, it is often desirable to produce multiple Rayleigh fading processes with given frequency correlation properties. In this paper, a novel stochastic wide-sense stationary sum-of-sinusoids channel simulator is proposed to emulate frequency-correlated wideband fading channels, where the frequency correlation properties are controlled by only adjusting the constant phases. Closed-form expressions are provided for all the parameters of the simulation model. This enables us to investigate analytically the overall correlation properties (not only the correlation coefficients) of the simulated processes with respect to both time separation and frequency separation. It is shown that the wideband channel simulator will be reduced to a narrowband Rayleigh fading-channel simulator by removing the frequency selectivity. Furthermore, the COST 207 typical-urban and rural-area channels are applied to evaluate the performance of the resulting wideband and narrowband channel simulators, respectively. The correlation properties of the simulation models approach the desired ones of the underlying reference models as the number of exponential functions tends to infinity, while very good approximations are achieved with the chosen limited number of exponential functions.

Index Terms—Frequency correlation, Rayleigh fading channels, statistics, stochastic sum-of-sinusoids channel simulators, wideband fading channels.

I. INTRODUCTION

MULTIPLE correlated Rayleigh fading signals are commonly encountered in frequency-diversity wireless-communication systems, such as frequency-hopping (FH) systems, multicarrier code-division multiple-access (MC-CDMA) systems, and orthogonal frequency-division multiplexing (OFDM) systems. For convenience, researchers investigating these systems have typically assumed that the frequency separation of two signals at different carrier frequencies is sufficiently large compared with the coherence bandwidth of the channel. This assumption implies that the fading characteristics of dif-

ferent frequency-separated channels are uncorrelated [1], and therefore, the underlying channel simulator can be implemented by using uncorrelated fading processes. However, in practical frequency-diversity systems, the frequency separation of different channels is often smaller than the coherence bandwidth due to spectrum and frequency planning constraints [2]–[8]. In this case, the frequency correlation will exist among different channels, resulting in the so-called frequency-correlated channels. Since the assumption of uncorrelated fading does not take the frequency correlation into account, positively biased performance results are often obtained for the investigated systems. Therefore, accurate theoretical analyses and simulations of multiple frequency-correlated Rayleigh fading channels are of great importance in investigating the influence of the frequency correlation on the performance of real frequency-diversity systems.

In the literature, different algorithms have been presented for the generation of two [4] or any number [5]–[8] of frequency-correlated Rayleigh fading processes. The authors of [4]–[8] have all employed the method of generating correlated processes by using a linear transformation of uncorrelated processes. To this end, multiple uncorrelated processes must first be produced, and the Cholesky decomposition technique has to be used to factorize the given correlation coefficient matrix [4]–[8]. This significantly increases the complexity and restrict the application of the algorithms [4]–[8] to real systems, particularly when the required number of correlated processes is large. Furthermore, the papers in [4]–[8] have only studied the correlation coefficients of the generated processes and not the overall correlation properties with respect to both time separation and frequency separation.

The sum-of-sinusoids approach [9], [10] is well known to be an efficient and flexible method for the simulation of mobile fading channels. Its application to the design of fading-channel simulators includes the modeling of narrowband channels [1], [11], wideband channels [11]–[14], spatial-temporal channels [15], [16], and digital channels (generative models) [17], [18]. For the purpose of simulating space diversity channels and multiple-input-multiple-output channels, the sum-of-sinusoids method has also been widely employed to generate multiple uncorrelated [19]–[23] and correlated [24] Rayleigh fading processes. However, the channel simulators described in the study in [19]–[24] cannot be directly applied to the simulation of frequency-correlated Rayleigh fading channels. Based on the same mathematical reference model, as described in the

Manuscript received December 22, 2003; revised November 24, 2004, January 23, 2006, April 11, 2006, and May 29, 2006. The review of this paper was coordinated by Prof. A. Abdi.

C.-X. Wang is with Joint Research Institute of Signal and Image Processing, School of Engineering and Physical Sciences, Heriot-Watt University, EH14 4AS Edinburgh, U.K. (e-mail: cheng-xiang.wang@hw.ac.uk).

M. Pätzold and Q. Yao are with the Faculty of Engineering and Science, Agder University College, 4876 Grimstad, Norway (e-mail: matthias.patzold@hia.no; qi.yao2001@hotmail.com).

Digital Object Identifier 10.1109/TVT.2007.895490

study in [1], two deterministic sum-of-sinusoids channel simulators [25], [26] have been developed to model FH Rayleigh fading channels with given frequency correlation properties. Although not explicitly indicated in the study in [25] and [26], these two channel simulators can also be used to simulate other frequency-diversity channels, such as MC-CDMA and OFDM channels. Unfortunately, there still exist relatively large deviations between some of the statistical properties of both channel simulators [25], [26] and those of the underlying reference model [1]. Moreover, these two channel simulators are limited to model only narrowband channels, where the transmitted symbol rate is much smaller than the channel coherence bandwidth. Modern frequency-diversity wireless-communication systems are often designed for high symbol rates. If the symbol rate is so high as in the order of the coherence bandwidth, the channel becomes wideband or frequency selective. The aim of this paper is to develop a stochastic sum-of-sinusoids channel simulator that can simulate multiple frequency-correlated wideband fading channels with accurate statistical properties.

For our purpose, a mathematical reference model based on the tapped-delay-line structure [27], [28] is first presented in modeling frequency-correlated wideband fading channels. In order to be consistent with the study in [1], we have assumed a 2-D isotropic scattering propagation environment with omnidirectional antennas at receivers [29] and a truncated negative exponential power delay profile (PDP). It is important to mention that a different profile, e.g., the Gaussian function [14], can also be deployed as the PDP. The application of the present modeling procedure to different PDPs is straightforward. The overall correlation properties among different frequency-separated channels are investigated in detail with respect to both time separation and frequency separation. By removing the frequency selectivity from the proposed wideband reference model, it is shown that the derived correlation functions will be reduced to the results presented in [1, p. 50] for narrowband Rayleigh fading channels. Hence, the narrowband reference model in [1, p. 48] is only a special case of the proposed wideband reference model. Then, we propose a novel stochastic sum-of-sinusoids simulation model, which can emulate accurately all of the correlation properties of the derived wideband reference model. Similarly, a narrowband Rayleigh fading channel simulator can be obtained by removing the frequency selectivity from the wideband simulation model. Rather than first generating uncorrelated processes, as in [4]–[8] and [24], the proposed channel simulator can directly simulate multiple frequency-correlated processes by only adjusting the constant phases of the employed harmonic functions. The stationarity properties of stochastic sum-of-sinusoids channel simulators have recently been addressed in several papers, e.g., in [30]–[32]. We will show that the proposed stochastic channel simulator is wide-sense stationary (WSS).

The remainder of this paper is organized as follows. In Section II, a reference model for frequency-correlated wideband fading channels is proposed. It is shown that the wideband reference model will be reduced to the narrowband reference model in [1] by removing the frequency selectivity. A novel stochastic sum-of-sinusoids-based wideband channel simulator

is described in Section III. In this section, we also show how the model parameters can be determined. Section IV deals with the performance evaluation and verification of the proposed simulation model. Finally, the conclusions are drawn in Section V.

II. MATHEMATICAL REFERENCE MODEL

A. Reference Model for Frequency-Correlated Wideband Fading Channels

Bello's WSS uncorrelated-scattering (WSSUS) model [33] has widely been accepted in modeling wideband multipath fading channels. Regarding the design of hardware or software simulation models for wideband channels, a discretization of the propagation delays has to be performed. A suitable and often used model is the so-called discrete tapped-delay-line model [27], [28]. It is important to mention that a discrete tapped-delay-line model is a WSSUS model if the time-variant tap coefficients are uncorrelated Gaussian random processes. The complex baseband impulse responses at two different carrier frequencies f_c and f_c^\dagger can be expressed as

$$h(\tau', t) := \sum_{\ell=0}^{\mathcal{L}-1} \mu_\ell(t) \delta(\tau' - \tau'_\ell), \text{ at } f_c \quad (1a)$$

$$h^\dagger(\tau', t) := \sum_{\ell=0}^{\mathcal{L}-1} \mu_\ell^\dagger(t) \delta(\tau' - \tau'_\ell), \text{ at } f_c^\dagger \quad (1b)$$

where \mathcal{L} is the number of taps, and $\mu_\ell(t)$ ($\mu_\ell^\dagger(t)$) and τ'_ℓ indicate the complex time-variant tap coefficient and the discrete propagation delay of the ℓ th ($\ell = 0, 1, \dots, \mathcal{L} - 1$) tap, respectively. According to the authors of [14] and [34], a proper PDP $p(\tau')$ for a wideband channel is given by the following truncated negative exponential profile:

$$p(\tau') = \frac{b}{\alpha} \exp\left(-\frac{\tau'}{\alpha}\right), \quad 0 \leq \tau' \leq \tau'_{\max} \quad (2)$$

where α represents the rms delay spread, and τ'_{\max} denotes the maximum propagation delay. The normalization factor $b = 1/(1 - e^{-\tau'_{\max}/\alpha})$ has been introduced here to fulfill the condition $\int_0^{\tau'_{\max}} p(\tau') d\tau' = 1$. This means that the average power of the wideband fading channel is normalized to unity, and hence, the PDP in (2) can be considered as the probability density function (pdf) of the propagation delays. An example of (2) is given by $\alpha = 1 \mu\text{s}$ and $\tau'_{\max} = 7 \mu\text{s}$. In this case, the PDP of the wideband typical-urban (TU) channel for global system for mobile communications (GSM) is obtained [34]. The frequency correlation function (FCF) $R(\chi)$ is related to the PDP through the Fourier transform [33], i.e.,

$$R(\chi) = \int_0^{\tau'_{\max}} p(\tau') \exp(-j2\pi\tau'\chi) d\tau' \\ = \frac{b \left\{ 1 - \exp\left[-\frac{\tau'_{\max}}{\alpha} (1 + j2\pi\alpha\chi)\right] \right\}}{1 + j2\pi\alpha\chi}. \quad (3)$$

For a discrete tapped-delay-line model, each tap is considered as the combination of a number of multipath components. The propagation delay interval $I = [0, \tau'_{\max}]$ is partitioned into \mathcal{L} mutually disjoint subintervals I_ℓ , i.e., $I = \cup_{\ell=0}^{\mathcal{L}-1} I_\ell$ and $I_\ell \cap I_\lambda = \{\emptyset\}$ for every ℓ and $\lambda \neq \ell$ ($\ell, \lambda = 0, 1, \dots, \mathcal{L} - 1$) [13], [14]. Each subinterval I_ℓ corresponds to the range within which a number of multipath components are combined to the ℓ th tap. For simplicity, the subintervals I_ℓ can be defined as follows:

$$I_\ell = \begin{cases} [\tau'_\ell - \Delta\tau'_\ell/2, \tau'_\ell + \Delta\tau'_{\ell+1}/2), & \ell = 0, 1, \dots, \mathcal{L} - 2 \\ [\tau'_\ell - \Delta\tau'_\ell/2, \tau'_\ell + \Delta\tau'_{\ell+1}/2], & \ell = \mathcal{L} - 1 \end{cases} \quad (4)$$

where $\Delta\tau'_0 = \tau'_0 = 0$, $\Delta\tau'_\ell = \tau'_\ell - \tau'_{\ell-1}$ ($\ell = 1, 2, \dots, \mathcal{L} - 1$), and $\Delta\tau'_\mathcal{L} = 2(\tau'_{\max} - \tau'_{\mathcal{L}-1})$. The above expression can be rewritten as

$$I_\ell = \begin{cases} [0, \Delta\tau'_{\ell+1}/2), & \ell = 0 \\ [\tau'_\ell - \Delta\tau'_\ell/2, \tau'_\ell + \Delta\tau'_{\ell+1}/2), & \ell = 1, 2, \dots, \mathcal{L} - 2 \\ [\tau'_\ell - \Delta\tau'_\ell/2, \tau'_{\max}], & \ell = \mathcal{L} - 1 \end{cases} \quad (5)$$

Note that the time-variant tap coefficient $\mu_\ell(t)$ corresponding to the discrete propagation delay τ'_ℓ actually stands for the contribution of the channel impulse response $h(\tau', t)$ in the interval $\tau' \in I_\ell$, i.e., $\mu_\ell(t) = \int_{\tau' \in I_\ell} h(\tau', t) d\tau'$. By analogy, $\mu_\ell^\dagger(t) = \int_{\tau' \in I_\ell} h^\dagger(\tau', t) d\tau'$ holds. It is important to stress here that the delay spacing between the taps should be chosen to avoid a regular spacing, i.e., $\Delta\tau'_\ell \neq \Delta\tau'_{\ell+1}$. This is to ensure the FCF of the radio channel has a sufficiently large period (at least larger than twice the system bandwidth), which is particularly important for FH systems.

Under the WSSUS condition, the time-variant tap coefficients $\mu_\ell(t)$ and $\mu_\ell^\dagger(t)$ are zero-mean complex Gaussian random processes. It follows that the amplitude processes $|\mu_\ell(t)|$ and $|\mu_\ell^\dagger(t)|$ are Rayleigh distributed. The Central-Limit Theorem [36] justifies that a Gaussian random process can be modeled by a superposition of an infinite number of properly weighted sinusoids. Therefore, we propose to model $\mu_\ell(t)$ and $\mu_\ell^\dagger(t)$ as

$$\begin{aligned} \mu_\ell(t) &= \mu_{1,\ell}(t) + j\mu_{2,\ell}(t) \\ &= \lim_{\substack{N_\ell \rightarrow \infty \\ M_\ell \rightarrow \infty}} \sum_{n=1}^{N_\ell} \sum_{m=1}^{M_\ell} C_{n,m,\ell} \\ &\quad \times \exp \left[j \left(2\pi f_{\max} t \cos \beta_{n,\ell} - \Phi_{n,m,\ell} - \hat{\theta}_{n,m,\ell} \right) \right] \quad (6a) \end{aligned}$$

$$\begin{aligned} \mu_\ell^\dagger(t) &= \mu_{1,\ell}^\dagger(t) + j\mu_{2,\ell}^\dagger(t) \\ &= \lim_{\substack{N_\ell \rightarrow \infty \\ M_\ell \rightarrow \infty}} \sum_{n=1}^{N_\ell} \sum_{m=1}^{M_\ell} C_{n,m,\ell} \\ &\quad \times \exp \left[j \left(2\pi f_{\max} t \cos \beta_{n,\ell} - \Phi_{n,m,\ell}^\dagger - \hat{\theta}_{n,m,\ell} \right) \right] \quad (6b) \end{aligned}$$

with $\Phi_{n,m,\ell} = 2\pi f_c \varphi_{n,m,\ell}$ and $\Phi_{n,m,\ell}^\dagger = 2\pi f_c^\dagger \varphi_{n,m,\ell}$. Here, f_{\max} is the maximum Doppler frequency, and $C_{n,m,\ell}$, $\beta_{n,\ell}$, and $\varphi_{n,m,\ell}$ are independent random gains, random angles of arrival, and random propagation delays of the ℓ th tap, respectively. The phases $\hat{\theta}_{n,m,\ell}$ are independent random variables uniformly distributed over $[0, 2\pi)$. Equations (6a) and (6b) can be interpreted as follows. For the diffuse components $\mu_\ell(t)$ ($\mu_\ell^\dagger(t)$) of the ℓ th tap, the n th wave at the angle of arrival $\beta_{n,\ell}$ is also composed of M_ℓ waves with amplitudes $C_{n,m,\ell}$ and propagation delays $\varphi_{n,m,\ell} \in I_\ell$. All of these M_ℓ waves experience the same Doppler shift $f_{\max} \cos \beta_{n,\ell}$. Adopting Clarke's 2-D isotropic scattering model [29], the angles of arrival $\beta_{n,\ell}$ are uniformly distributed over $[0, 2\pi)$, i.e., $p(\beta) = 1/(2\pi)$, $0 \leq \beta < 2\pi$. The average fractional power of the ℓ th tap as a function of propagation delays $\varphi_{n,m,\ell}$ still follows the truncated negative exponential profile introduced in (2), i.e.,

$$p(\varphi) = \frac{b}{\alpha} \exp\left(-\frac{\varphi}{\alpha}\right), \quad \varphi \in I_\ell. \quad (7)$$

Clearly, $\int_0^{\tau'_{\max}} p(\tau') d\tau' = \sum_{\ell=0}^{\mathcal{L}-1} \int_{\varphi \in I_\ell} p(\varphi) d\varphi = 1$ holds. The random gains $C_{n,m,\ell}$ can be related to the power associated with each individual wave of the ℓ th tap as follows: $C_{n,m,\ell}^2 = p(\beta_{n,\ell}, \varphi_{n,m,\ell}) d\beta d\varphi$ [1]. Note that $p(\beta, \varphi) d\beta d\varphi$ describes the fraction of the incoming power within the infinitesimal intervals $d\beta$ and $d\varphi$.

From (6), it follows that the correlation properties of $\mu_\ell(t)$ and $\mu_\lambda^\dagger(t)$ ($\ell, \lambda = 0, 1, \dots, \mathcal{L} - 1$) are completely determined by the underlying real Gaussian noise processes $\mu_{i,\ell}(t)$ and $\mu_{j,\lambda}^\dagger(t)$ ($i, j = 1, 2$). Therefore, we can restrict our investigations to the following autocorrelation functions (ACFs) and cross-correlation functions (CCFs):

$$r_{\mu_{i,\ell}\mu_{j,\lambda}}(\tau) := E \{ \mu_{i,\ell}(t) \mu_{j,\lambda}(t + \tau) \} \quad (8a)$$

$$r_{\mu_{i,\ell}\mu_{j,\lambda}^\dagger}(\tau, \chi) := E \{ \mu_{i,\ell}(t) \mu_{j,\lambda}^\dagger(t + \tau) \} \quad (8b)$$

where $E\{\cdot\}$ denotes the statistical average with respect to $\beta_{n,\ell}$, $\varphi_{n,m,\ell}$, and $\hat{\theta}_{n,m,\ell}$. It should be observed that (8b) is a function of both time separation $\tau = t_2 - t_1$ and frequency separation $\chi = f_c^\dagger - f_c$. Using (6), we can obtain the following correlation functions of the wideband reference model:

$$\begin{aligned} r_{\mu_{i,\ell}\mu_{i,\ell}}(\tau) &= r_{\mu_{i,\ell}^\dagger\mu_{i,\ell}^\dagger}(\tau) \\ &= \frac{1}{2} b(A_\ell - B_\ell) J_0(2\pi f_{\max} \tau) \quad (9a) \end{aligned}$$

$$\begin{aligned} r_{\mu_{1,\ell}\mu_{2,\ell}}(\tau) &= r_{\mu_{1,\ell}^\dagger\mu_{2,\ell}^\dagger}(\tau) \\ &= r_{\mu_{2,\ell}\mu_{1,\ell}}(\tau) \\ &= r_{\mu_{2,\ell}^\dagger\mu_{1,\ell}^\dagger}(\tau) \\ &= 0 \quad (9b) \end{aligned}$$

$$\begin{aligned} r_{\mu_{i,\ell}\mu_{j,\lambda}}(\tau) &= r_{\mu_{i,\ell}^\dagger\mu_{j,\lambda}^\dagger}(\tau) \\ &= 0 \quad (9c) \end{aligned}$$

$$r_{\mu_{i,\ell}\mu_{i,\ell}^\dagger}(\tau, \chi) = \frac{bJ_0(2\pi f_{\max}\tau)}{2[1 + (2\pi\alpha\chi)^2]} \exp\left(-\frac{\varphi}{\alpha}\right) \\ \times [2\pi\alpha\chi \sin(2\pi\chi\varphi) - \cos(2\pi\chi\varphi)] \Big|_{\varphi=\tau'_\ell - \Delta\tau'_\ell/2}^{\varphi=\tau'_\ell + \Delta\tau'_{\ell+1}/2} \quad (9d)$$

$$r_{\mu_{1,\ell}\mu_{2,\ell}^\dagger}(\tau, \chi) = -r_{\mu_{2,\ell}\mu_{1,\ell}^\dagger}(\tau, \chi) \\ = \frac{bJ_0(2\pi f_{\max}\tau)}{2[1 + (2\pi\alpha\chi)^2]} \exp\left(-\frac{\varphi}{\alpha}\right) \\ \times [\sin(2\pi\chi\varphi) + 2\pi\alpha\chi \\ \times \cos(2\pi\chi\varphi)] \Big|_{\varphi=\tau'_\ell - \Delta\tau'_\ell/2}^{\varphi=\tau'_\ell + \Delta\tau'_{\ell+1}/2} \quad (9e)$$

$$r_{\mu_{i,\ell}\mu_{j,\lambda}^\dagger}(\tau, \chi) = 0 \quad (9f)$$

for $i, j = 1, 2$ and $\ell, \lambda = 0, 1, \dots, \mathcal{L} - 1$ with $\ell \neq \lambda$, where $J_0(\cdot)$ denotes the zeroth-order Bessel function of the first kind, $A_\ell = \exp[-(\tau'_\ell - \Delta\tau'_\ell/2)/\alpha]$, and $B_\ell = \exp[-(\tau'_\ell + \Delta\tau'_{\ell+1}/2)/\alpha]$. In (9d) and (9e), $f(x)|_{x=x_1}^{x=x_2}$ is an abbreviation for $f(x_2) - f(x_1)$. Since the derivations of (9a)–(9f) are similar, only the derivation of (9e) is given in Appendix A, while others are omitted here for brevity. The delay power Ω_ℓ assigned to the ℓ th tap can be obtained from (9a) according to $\Omega_\ell = 2r_{\mu_{i,\ell}\mu_{i,\ell}}(0) = b(A_\ell - B_\ell)$. The total delay power is, therefore, $\Omega_p = \sum_{\ell=0}^{\mathcal{L}-1} \Omega_\ell = 1$. The expression (9b) clearly indicates the uncorrelatedness between the in-phase and quadrature components of $\mu_\ell(t)$ ($\mu_\ell^\dagger(t)$). The expressions (9c) and (9f) state that there are no cross correlations between the underlying processes in different taps due to the uncorrelated-scattering (US) condition imposed on the model. From (9d) and (9e), it is clear that $r_{\mu_{i,\ell}\mu_{i,\ell}^\dagger}(\tau, \chi)$ and $r_{\mu_{1,\ell}\mu_{2,\ell}^\dagger}(\tau, \chi)$ are separable into two parts—one depends on the time-separation variable τ and the other one on the frequency-separation variable χ . Therefore, we can write $r_{\mu_{i,\ell}\mu_{i,\ell}^\dagger}(\tau, \chi) = r_{\mu_i\mu_i}(\tau)R_{\mu_{i,\ell}\mu_{i,\ell}^\dagger}(\chi)$ and $r_{\mu_{1,\ell}\mu_{2,\ell}^\dagger}(\tau, \chi) = r_{\mu_1\mu_1}(\tau)R_{\mu_{1,\ell}\mu_{2,\ell}^\dagger}(\chi)$, where $r_{\mu_i\mu_i}(\tau) = \sum_{\ell=0}^{\mathcal{L}-1} r_{\mu_{i,\ell}\mu_{i,\ell}}(\tau) = J_0(2\pi f_{\max}\tau)$. We can easily calculate $R_{\mu_{i,\ell}\mu_{i,\ell}^\dagger}(\chi)$ and $R_{\mu_{1,\ell}\mu_{2,\ell}^\dagger}(\chi)$ using (9d) and (9e), respectively. It can be shown further that $R_{\mu_{i,\ell}\mu_{i,\ell}^\dagger}(\chi)$ and $R_{\mu_{1,\ell}\mu_{2,\ell}^\dagger}(\chi)$ are related to the FCF $R(\chi)$ in (3) as follows:

$$R(\chi) = \sum_{\ell=0}^{\mathcal{L}-1} \left[R_{\mu_{i,\ell}\mu_{i,\ell}^\dagger}(\chi) + jR_{\mu_{1,\ell}\mu_{2,\ell}^\dagger}(\chi) \right]. \quad (10)$$

B. Reference Model for Frequency-Correlated Narrowband Rayleigh Fading Channels

A special case of the wideband channel model described by (1) is given when $\mathcal{L} = 1$. Consequently, $h(\tau', t) = \mu(t)\delta(\tau')$ and $h^\dagger(\tau', t) = \mu^\dagger(t)\delta(\tau')$ hold. These are actually the impulse responses of a narrowband-channel model. To make this evident, we express the stochastic processes $\mu(t)$ and

$\mu^\dagger(t)$ similarly to (6a) and (6b) by removing the subscript $(\cdot)_\ell$, i.e.,

$$\mu(t) = \mu_1(t) + j\mu_2(t) \\ = \lim_{\substack{N \rightarrow \infty \\ M \rightarrow \infty}} \sum_{n=1}^N \sum_{m=1}^M C_{n,m} \\ \times \exp\left[j\left(2\pi f_{\max}t \cos \beta_n - \Phi_{n,m} - \hat{\theta}_{n,m}\right)\right] \quad (11a)$$

$$\mu^\dagger(t) = \mu_1^\dagger(t) + j\mu_2^\dagger(t) \\ = \lim_{\substack{N \rightarrow \infty \\ M \rightarrow \infty}} \sum_{n=1}^N \sum_{m=1}^M C_{n,m} \\ \times \exp\left[j\left(2\pi f_{\max}t \cos \beta_n - \Phi_{n,m}^\dagger - \hat{\theta}_{n,m}\right)\right] \quad (11b)$$

with $\Phi_{n,m} = 2\pi f_c \varphi_{n,m}$ and $\Phi_{n,m}^\dagger = 2\pi f_c^\dagger \varphi_{n,m}$. In order to be consistent with [1], we employ for the narrowband-channel model a negative exponential PDP, i.e.,

$$p(\varphi) = \frac{1}{\alpha} \exp\left(-\frac{\varphi}{\alpha}\right), \quad \varphi \geq 0 \quad (12)$$

which is a special case of the truncated exponential PDP in (2) for $\tau'_{\max} \rightarrow \infty$. Again, the PDP in (12) can actually be regarded as the pdf of the propagation delays, since the average power of the narrowband fading channel is normalized to be one, i.e., $\int_0^\infty p(\varphi)d\varphi = 1$ holds. Note that the value of α in (12) must be much less than the symbol duration for a narrowband channel. An example is the rural-area (RA) channel model [34] developed for GSM, where $\alpha = 0.1086 \mu\text{s}$, and the symbol duration is about $3.7 \mu\text{s}$. By taking the Fourier transform of the PDP in (12), the FCF is given by

$$R(\chi) = \frac{1}{1 + j2\pi\alpha\chi}. \quad (13)$$

The correlation properties of the above narrowband-channel model can be easily obtained from (9) by neglecting the subscript $(\cdot)_\ell$. In this case, $\tau'_\ell - \Delta\tau'_\ell/2 = 0$, and $\tau'_\ell + \Delta\tau'_{\ell+1}/2 = \tau'_{\max} \rightarrow \infty$, i.e., $A_0 = 1$, $B_0 = 0$, and $b = 1$ hold. The resulting correlation functions are given by

$$r_{\mu_i\mu_i}(\tau) = r_{\mu_i^\dagger\mu_i^\dagger}(\tau) \\ = \frac{1}{2} J_0(2\pi f_{\max}\tau) \quad (14a)$$

$$r_{\mu_1\mu_2}(\tau) = r_{\mu_1^\dagger\mu_2^\dagger}(\tau) \\ = r_{\mu_2\mu_1}(\tau) \\ = r_{\mu_2^\dagger\mu_1^\dagger}(\tau) \\ = 0 \quad (14b)$$

$$r_{\mu_i\mu_i^\dagger}(\tau, \chi) = \frac{J_0(2\pi f_{\max}\tau)}{2[1 + (2\pi\alpha\chi)^2]} \quad (14c)$$

$$r_{\mu_1\mu_2^\dagger}(\tau, \chi) = -r_{\mu_2\mu_1^\dagger}(\tau, \chi) \\ = -2\pi\alpha\chi r_{\mu_i\mu_i^\dagger}(\tau, \chi). \quad (14d)$$

As investigated in the study in [4]–[8] and [24], the correlation coefficients of the corresponding stochastic processes can easily be gained by evaluating the correlation functions in (14) at $\tau = 0$. The separability property of $r_{\mu_i\mu_i^\dagger}(\tau, \chi)$ is clear from

the following expression: $r_{\mu_i \mu_i^\dagger}(\tau, \chi) = r_{\mu_i \mu_i}(\tau) R_{\mu_i \mu_i^\dagger}(\chi)$, where $R_{\mu_i \mu_i^\dagger}(\chi) = 1/[1 + (2\pi\alpha\chi)^2]$. Similarly, $r_{\mu_1 \mu_2^\dagger}(\tau, \chi) = r_{\mu_1 \mu_2}(\tau) R_{\mu_1 \mu_2^\dagger}(\chi)$ holds, where $R_{\mu_1 \mu_2^\dagger}(\chi) = -2\pi\alpha\chi/[1 + (2\pi\alpha\chi)^2]$. A close comparison of $R_{\mu_i \mu_i^\dagger}(\chi)$, $R_{\mu_1 \mu_2^\dagger}(\chi)$, and the FCF $R(\chi)$ in (13) gives the following relation: $R(\chi) = R_{\mu_i \mu_i^\dagger}(\chi) + jR_{\mu_1 \mu_2^\dagger}(\chi)$.

Note that the frequency-correlated narrowband Rayleigh fading channel model described by (11) is essentially the same as the equivalent baseband-channel model given in [1, p. 48]. As a result, the correlation functions in (14) are in agreement with those presented in [1, p. 50], as well as in [25] and [26]. Therefore, the proposed wideband-channel model described by (1) and (6) includes the narrowband-channel model in [1, p. 48] as a special case if the (truncated) negative exponential PDP is employed. However, the proposed modeling procedure can also be applied to other forms of PDP, e.g., as shown in [14].

It should be clarified at this point that the mathematical model described by (1) and (6), as well as its special case described by (12), stands for a nonrealizable stochastic reference model, since the employed numbers of exponential functions tend to infinity. Nevertheless, the correlation functions shown in (9a)–(9f) and (14a)–(14d) provide the basis for the performance evaluation of the realizable simulation model described in the next section.

III. NOVEL STOCHASTIC SUM-OF-SINUSOIDS SIMULATION MODEL

A. Simulation Model for Frequency-Correlated Wideband Fading Channels

The stochastic simulation model proposed here is also based on the discrete tapped-delay-line structure as in the reference model, but the manner how the complex random processes are modeled is completely different. The impulse responses of the simulation model are again composed of \mathcal{L} discrete taps according to

$$\hat{h}(\tau', t) := \sum_{\ell=0}^{\mathcal{L}-1} \hat{\mu}_\ell(t) \delta(\tau' - \tau'_\ell), \text{ at } f_c \quad (15a)$$

$$\hat{h}^\dagger(\tau', t) := \sum_{\ell=0}^{\mathcal{L}-1} \hat{\mu}_\ell^\dagger(t) \delta(\tau' - \tau'_\ell), \text{ at } f_c^\dagger \quad (15b)$$

where the discrete propagation delays τ'_ℓ are identical to those of the reference model. Concerning the simulation model, it is important to mention that τ'_ℓ must be an integer multiple of the sampling interval T'_s , i.e., $\tau'_\ell = q_\ell \cdot T'_s$, with q_ℓ denoting a non-negative integer. Given τ'_ℓ , T'_s can be determined by $T'_s = \text{gcd}\{\tau'_\ell\}_{\ell=1}^{\mathcal{L}-1}$, where $\text{gcd}\{\cdot\}$ represents the greatest common divisor [11]. In case that the original simulation sampling interval is so large that the discrete propagation delays τ'_ℓ are not multiples of the sampling interval, it is necessary to increase the sampling rate (up-sampling) to accommodate all the different discrete delays. This will reduce the simulation speed and result in computationally inefficient simulations. To solve this problem, several conversion methods were discussed in the

study in [35] to use an alternative model from the original one having all discrete propagation delays matching the sampling interval without using up-sampling techniques.

In (15a) and (15b), the stochastic processes $\hat{\mu}_\ell(t)$ and $\hat{\mu}_\ell^\dagger(t)$ are modeled by a finite double sum of properly weighted exponential functions

$$\begin{aligned} \hat{\mu}_\ell(t) &= \hat{\mu}_{1,\ell}(t) + j\hat{\mu}_{2,\ell}(t) \\ &= \sum_{n=-N_\ell+1}^{N_\ell} \sum_{m=1}^{M_\ell} c_{n,m,\ell} \exp\left[j\left(2\pi f_{n,\ell} t - \theta_{m,\ell} - \hat{\theta}_{n,m,\ell}\right)\right] \end{aligned} \quad (16a)$$

$$\begin{aligned} \hat{\mu}_\ell^\dagger(t) &= \hat{\mu}_{1,\ell}^\dagger(t) + j\hat{\mu}_{2,\ell}^\dagger(t) \\ &= \sum_{n=-N_\ell+1}^{N_\ell} \sum_{m=1}^{M_\ell} c_{n,m,\ell} \exp\left[j\left(2\pi f_{n,\ell} t - \theta_{m,\ell}^\dagger - \hat{\theta}_{n,m,\ell}\right)\right] \end{aligned} \quad (16b)$$

with $\theta_{m,\ell} = 2\pi f_c \phi_{m,\ell}$, and $\theta_{m,\ell}^\dagger = 2\pi f_c^\dagger \phi_{m,\ell}$. Here, $2N_\ell M_\ell$ defines the finite number of exponential functions of the ℓ th tap, mainly determining the realization expenditure and the performance of the resulting channel simulator. The gains $c_{n,m,\ell}$, the discrete Doppler frequencies $f_{n,\ell}$, and the discrete delays $\phi_{m,\ell}$ will be determined during the simulation-setup phase and kept constant during simulation. The phases $\hat{\theta}_{n,m,\ell}$ are independent random variables uniformly distributed in the interval $[0, 2\pi)$. The expressions (16a) and (16b) provide us with further observations: When different carrier frequencies f_c and $f_c^\dagger = f_c + \chi$ are employed in the physical channel model, we only have to adopt the corresponding sets of constant phases $\theta_{m,\ell}$ and $\theta_{m,\ell}^\dagger = \theta_{m,\ell} + 2\pi\chi\phi_{m,\ell}$ ($m = 1, 2, \dots, M_\ell$) in the simulation model, while maintaining all other parameters unchanged. Therefore, this channel simulator can directly simulate frequency-correlated processes by simply adjusting the constant phases, which is completely different from the method of generating correlated processes by using a linear transformation of uncorrelated processes in [4]–[8] and [24].

Following (15a), Fig. 1(a) shows the discrete tapped-delay-line structure of the resulting stochastic simulation model corresponding to the carrier frequency f_c . The input and output signals of the channel are represented here by $x(t)$ and $y(t)$, respectively. The structure of the underlying complex stochastic process $\hat{\mu}_\ell(t)$ [see (16a)] of the ℓ th ($\ell = 0, 1, \dots, \mathcal{L} - 1$) tap is illustrated in Fig. 1(b). By substituting in Fig. 1(b) the constant phases $\theta_{m,\ell}$ by $\theta_{m,\ell}^\dagger$, which performs the same function as we substitute in Fig. 1(a) $\hat{\mu}_\ell(t)$ by $\hat{\mu}_\ell^\dagger(t)$, we will immediately obtain a model corresponding to another carrier frequency f_c^\dagger [see (15b) and (16b)].

The correlation properties of the stochastic processes $\hat{\mu}_{i,\ell}(t)$ and $\hat{\mu}_{j,\lambda}^\dagger(t)$ ($i, j = 1, 2$ and $\ell, \lambda = 0, 1, \dots, \mathcal{L} - 1$) are calculated according to the following definitions:

$$\hat{r}_{\mu_{i,\ell} \mu_{j,\lambda}}(\tau) := E \left\{ \hat{\mu}_{i,\ell}(t) \hat{\mu}_{j,\lambda}(t + \tau) \right\} \quad (17a)$$

$$\hat{r}_{\mu_{i,\ell} \mu_{j,\lambda}^\dagger}(\tau, \chi) := E \left\{ \hat{\mu}_{i,\ell}(t) \hat{\mu}_{j,\lambda}^\dagger(t + \tau) \right\}. \quad (17b)$$

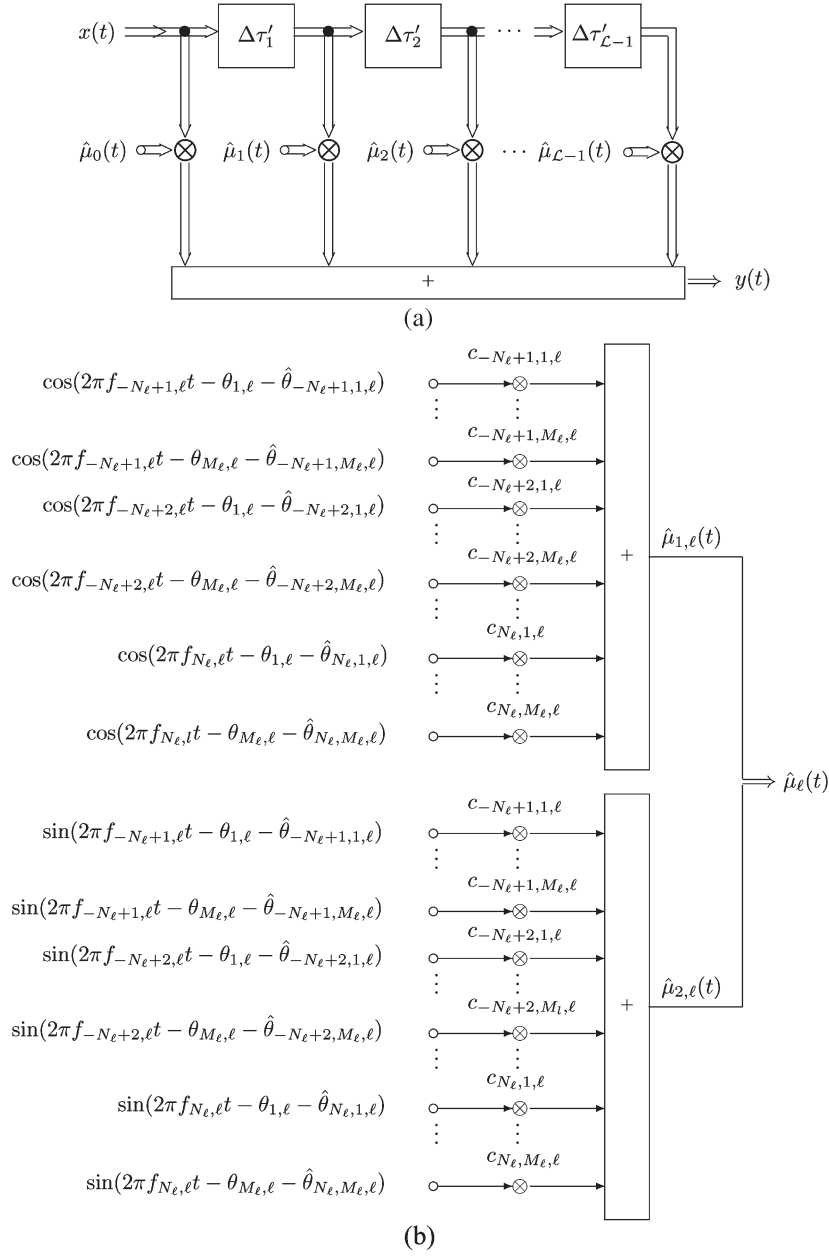


Fig. 1. Stochastic sum-of-sinusoids simulation model for wideband channels. (a) Discrete tapped-delay-line structure. (b) Underlying complex stochastic process $\hat{\mu}_\ell(t)$.

Here, $E\{\cdot\}$ indicates the statistical average with respect to the random phases $\hat{\theta}_{n,m,\ell}$. The substitution of (16) into (17) results in the following relations:

$$\begin{aligned} \hat{r}_{\mu_{i,\ell}\mu_{i,\ell}}(\tau) &= \hat{r}_{\mu_{i,\ell}^\dagger\mu_{i,\ell}^\dagger}(\tau) \\ &= \sum_{n=-N_\ell+1}^{N_\ell} \sum_{m=1}^{M_\ell} \frac{c_{n,m,\ell}^2}{2} \cos(2\pi f_{n,\ell}\tau) \end{aligned} \quad (18a)$$

$$\begin{aligned} \hat{r}_{\mu_{1,\ell}\mu_{2,\ell}}(\tau) &= \hat{r}_{\mu_{1,\ell}^\dagger\mu_{2,\ell}^\dagger}(\tau) \\ &= \hat{r}_{\mu_{2,\ell}\mu_{1,\ell}}(\tau) \\ &= \hat{r}_{\mu_{2,\ell}^\dagger\mu_{1,\ell}^\dagger}(\tau) \\ &= \sum_{n=-N_\ell+1}^{N_\ell} \sum_{m=1}^{M_\ell} \frac{c_{n,m,\ell}^2}{2} \sin(2\pi f_{n,\ell}\tau) \end{aligned} \quad (18b)$$

$$\begin{aligned} \hat{r}_{\mu_{i,\ell}\mu_{j,\ell}}(\tau) &= \hat{r}_{\mu_{i,\ell}^\dagger\mu_{j,\ell}^\dagger}(\tau) \\ &= 0 \end{aligned} \quad (18c)$$

$$\begin{aligned} \hat{r}_{\mu_{i,\ell}\mu_{i,\ell}}(\tau, \chi) &= \sum_{n=-N_\ell+1}^{N_\ell} \sum_{m=1}^{M_\ell} \frac{c_{n,m,\ell}^2}{2} \\ &\quad \cdot \cos(2\pi f_{n,\ell}\tau - 2\pi\phi_{m,\ell}\chi) \end{aligned} \quad (18d)$$

$$\begin{aligned} \hat{r}_{\mu_{1,\ell}\mu_{2,\ell}}(\tau, \chi) &= -\hat{r}_{\mu_{2,\ell}\mu_{1,\ell}}(\tau, \chi) \\ &= \sum_{n=-N_\ell+1}^{N_\ell} \sum_{m=1}^{M_\ell} \frac{c_{n,m,\ell}^2}{2} \\ &\quad \cdot \sin(2\pi f_{n,\ell}\tau - 2\pi\phi_{m,\ell}\chi) \end{aligned} \quad (18e)$$

$$\hat{r}_{\mu_{i,\ell}\mu_{j,\ell}}(\tau, \chi) = 0 \quad (18f)$$

for all $i, j = 1, 2$ and $\ell, \lambda = 0, 1, \dots, \mathcal{L} - 1$ with $\ell \neq \lambda$. Equation (18a) clearly states that the ACFs of $\hat{\mu}_{i,\ell}(t)$ and $\hat{\mu}_{i,\ell}^\dagger(t)$ depend only on the time separation $\tau = t_2 - t_1$. Moreover, it can be easily shown that the mean values of $\hat{\mu}_{i,\ell}(t)$ and $\hat{\mu}_{i,\ell}^\dagger(t)$ are equal to zero. According to the study in [36], a stochastic process is said to be WSS if its mean value is constant and its ACF depends only on the time separation τ . Therefore, $\hat{\mu}_{i,\ell}(t)$ and $\hat{\mu}_{i,\ell}^\dagger(t)$ are WSS processes. Consequently, the resulting stochastic channel simulator is WSS.

In the sequel, our aim is to find proper simulation model parameters in such a way that all of the correlation properties of the simulation model described by (18a)–(18f) will approximate as close as possible those of the given reference model described by (9a)–(9f). The gains $c_{n,m,\ell}$ and the discrete Doppler frequencies $f_{n,\ell}$ are derived by using the method of exact Doppler spread [11], which results in the following closed-form expressions:

$$c_{n,m,\ell} = \sqrt{\frac{b(A_\ell - B_\ell)}{2N_\ell M_\ell}} \quad (19a)$$

$$f_{n,\ell} = f_{\max} \sin \left[\frac{\pi}{2N_\ell} \left(n - \frac{1}{2} \right) \right] \quad (19b)$$

for $n = -N_\ell + 1, -N_\ell + 2, \dots, N_\ell$, $m = 1, 2, \dots, M_\ell$, and $\ell = 0, 1, \dots, \mathcal{L} - 1$. After substituting (19a) into (18a) and (18b), we realize that M_ℓ has no influence on $\hat{r}_{\mu_{i,\ell}\mu_{j,\ell}}(\tau)$ and $\hat{r}_{\mu_{i,\ell}\mu_{j,\ell}}(\tau)$. Moreover, the received power $\hat{\Omega}_\ell$ of the ℓ th tap can be obtained from (18a), according to $\hat{\Omega}_\ell = 2\hat{r}_{\mu_{i,\ell}\mu_{i,\ell}}(0) = b(A_\ell - B_\ell)$, which equals Ω_ℓ for the reference model. The substitution of (19a) and (19b) into (18b) makes clear that $\hat{r}_{\mu_{i,\ell}\mu_{j,\ell}}(\tau) = r_{\mu_{i,\ell}\mu_{j,\ell}}(\tau) = 0$ always holds for any given numbers of $N_\ell \geq 1$ and $M_\ell \geq 1$, since the $f_{n,\ell}$'s fulfill the following symmetry condition: $f_{-N_\ell+1,\ell} = -f_{N_\ell,\ell}, \dots, f_{0,\ell} = -f_{1,\ell}$. The symmetry property of $f_{n,\ell}$ is evidently illustrated in Fig. 2(a), where $f_{\max} = 91$ Hz and $N_\ell = 20$ were used as an example. Equation (19b) also states that the US condition [see (18c) and (18f)], which requires $f_{n,\ell} \neq \pm f_{k,\lambda}$ for $\ell \neq \lambda$, is always fulfilled in the case where $N_\ell/N_\lambda \neq (2n-1)/(2k-1)$ holds, where $n = 1, 2, \dots, N_\ell$ and $k = 1, 2, \dots, N_\lambda$ [23]. Concerning the computation of $\phi_{m,\ell}$ appearing in (18d) and (18e), the new method proposed in the study in [23] is applied in Appendix B, where the following closed-form expression is derived:

$$\phi_{m,\ell} = \alpha \ln \left[\frac{1}{A_\ell - \frac{m}{M_\ell}(A_\ell - B_\ell)} \right]. \quad (20)$$

Note that the discrete delays $\phi_{m,\ell}$ are located in the interval $(\tau'_\ell - \Delta\tau'_\ell/2, \tau'_\ell + \Delta\tau'_{\ell+1}/2]$, in which $\tau'_\ell - \Delta\tau'_\ell/2$ and $\tau'_\ell + \Delta\tau'_{\ell+1}/2$ correspond to $\phi_{0,\ell}$ and $\phi_{M_\ell,\ell}$, respectively. An example of $\phi_{m,\ell}$ with $\alpha = 1 \mu\text{s}$, $\ell = 0$ ($\tau'_0 = \Delta\tau'_0 = 0$), $\Delta\tau'_1 = 0.2 \mu\text{s}$, and $M_\ell = 20$ is plotted in Fig. 2(b). In this case, $\phi_{m,\ell} \in (0, 0.1] \mu\text{s}$ holds.

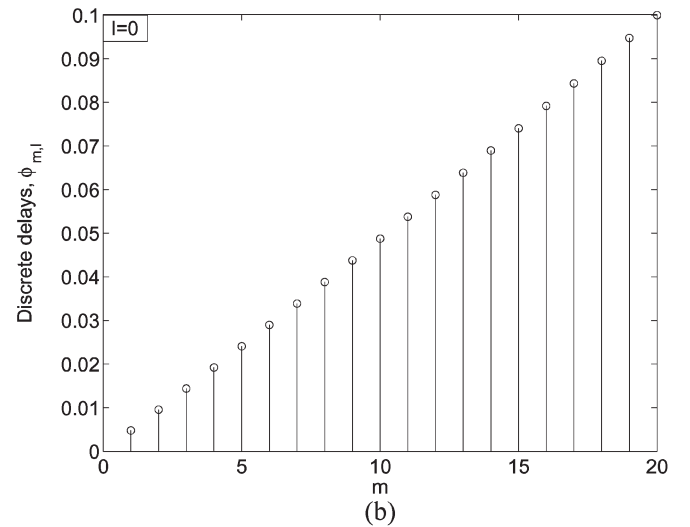
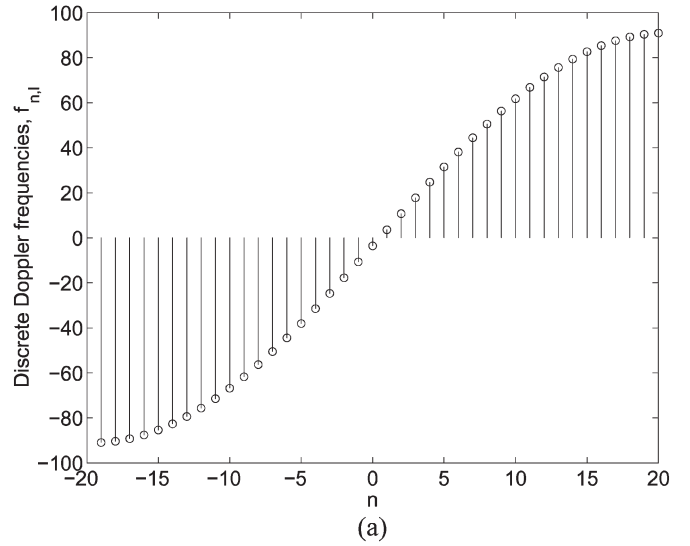


Fig. 2. (a) Discrete Doppler frequencies $f_{n,\ell}$ with $f_{\max} = 91$ Hz and $N_\ell = 20$. (b) Discrete delays $\phi_{m,\ell}$ with $\alpha = 1 \mu\text{s}$, $\ell = 0$ ($\tau'_0 = \Delta\tau'_0 = 0$), $\Delta\tau'_1 = 0.2 \mu\text{s}$, and $M_\ell = 20$.

B. Simulation Model for Frequency-Correlated Narrowband Rayleigh Fading Channels

Analogous to Section II-B, if we impose $\mathcal{L} = 1$ on the wideband simulation model in (15), it reduces to a narrowband Rayleigh fading channel simulator. It follows that $\hat{h}(\tau', t) = \hat{\mu}(t)\delta(\tau')$ and $\hat{h}^\dagger(\tau', t) = \hat{\mu}^\dagger(t)\delta(\tau')$ hold. The stochastic processes $\hat{\mu}(t)$ and $\hat{\mu}^\dagger(t)$ are then given by

$$\begin{aligned} \hat{\mu}(t) &= \hat{\mu}_1(t) + j\hat{\mu}_2(t) \\ &= \sum_{n=-N+1}^N \sum_{m=1}^M c_{n,m} \exp \left[j \left(2\pi f_n t - \theta_m - \hat{\theta}_{n,m} \right) \right] \end{aligned} \quad (21a)$$

$$\begin{aligned} \hat{\mu}^\dagger(t) &= \hat{\mu}_1^\dagger(t) + j\hat{\mu}_2^\dagger(t) \\ &= \sum_{n=-N+1}^N \sum_{m=1}^M c_{n,m} \exp \left[j \left(2\pi f_n t - \theta_m^\dagger - \hat{\theta}_{n,m} \right) \right] \end{aligned} \quad (21b)$$

with $\theta_m = 2\pi f_c \phi_m$ and $\theta_m^\dagger = 2\pi f_c^\dagger \phi_m$. The correlation properties of this narrowband simulation model can be obtained

from (18a)–(8f) by simply neglecting the subscript $(\cdot)_\ell$ in all the affected symbols. Thus

$$\begin{aligned}\hat{r}_{\mu_i\mu_i}(\tau) &= \hat{r}_{\mu_i^\dagger\mu_i^\dagger}(\tau) \\ &= \sum_{n=-N+1}^N \sum_{m=1}^M \frac{c_{n,m}^2}{2} \cos(2\pi f_n \tau)\end{aligned}\quad (22a)$$

$$\begin{aligned}\hat{r}_{\mu_1\mu_2}(\tau) &= \hat{r}_{\mu_1^\dagger\mu_2^\dagger}(\tau) \\ &= \hat{r}_{\mu_2\mu_1}(\tau) \\ &= \hat{r}_{\mu_2^\dagger\mu_1^\dagger}(\tau) \\ &= \sum_{n=-N+1}^N \sum_{m=1}^M \frac{c_{n,m}^2}{2} \sin(2\pi f_n \tau)\end{aligned}\quad (22b)$$

$$\hat{r}_{\mu_i\mu_i^\dagger}(\tau, \chi) = \sum_{n=-N+1}^N \sum_{m=1}^M \frac{c_{n,m}^2}{2} \cos(2\pi f_n \tau - 2\pi \phi_m \chi)\quad (22c)$$

$$\begin{aligned}\hat{r}_{\mu_1\mu_2^\dagger}(\tau, \chi) &= -\hat{r}_{\mu_2\mu_1^\dagger}(\tau, \chi) \\ &= \sum_{n=-N+1}^N \sum_{m=1}^M \frac{c_{n,m}^2}{2} \sin(2\pi f_n \tau - 2\pi \phi_m \chi).\end{aligned}\quad (22d)$$

If we remove the subscript $(\cdot)_\ell$ in (19) and (20) and further take into account $A_0 = 1$, $B_0 = 0$, and $b = 1$, all the parameters for the narrowband channel simulator are obtained as follows:

$$c_{n,m} = \frac{1}{\sqrt{2NM}}\quad (23a)$$

$$f_n = f_{\max} \sin \left[\frac{\pi}{2N} \left(n - \frac{1}{2} \right) \right]\quad (23b)$$

$$\phi_m = \alpha \ln \left(\frac{1}{1 - \frac{m-1/2}{M}} \right)\quad (24)$$

for $n = -N + 1, -N + 2, \dots, N$, and $m = 1, 2, \dots, M$. As shown in (24), we have substituted on the right-hand side the quantity m by $m - 1/2$ in order to avoid $\phi_m \rightarrow \infty$ when $m = M$.

It is important to point out that the derived correlation functions, as shown in (18a)–(18f) and (22a)–(22d), are always valid for the given simulation model [see (16) and (21)], while independent of any given reference model. However, the derived simulation-model parameters, as shown in (19), (20), (23), and (24), are only valid for the given reference model, where 2-D isotropic-scattering conditions and a (truncated) negative exponential PDP have been assumed. If the channel conditions of the reference model are different, the simulation model parameters have to be rederived.

IV. PERFORMANCE EVALUATION

The final acceptability of a novel channel simulator is usually established by analytical and numerical performance evalua-

tions. The extent to which the correlation properties of the proposed channel simulator and reference model agree will govern the degree of confidence we place in the modeling approach. In this section, we will validate the frequency-correlated wideband and narrowband Rayleigh fading channel simulators from both the analytical and simulation points of view.

A. Comparison of Correlation Functions for Wideband Fading Channels

The corresponding correlation functions of the wideband simulation model [see (18a)–(18f)] will be compared with those of the wideband reference model [see (9a)–(9f)]. As aforementioned in Section III-A, (18b), (18c), and (18f) are identical to (9b), (9c), and (9f), respectively. Moreover, by substituting (19a) and (19b) into (18a), we can show that the ACF $\hat{r}_{\mu_i, \ell \mu_i, \ell}(\tau)$ of the simulation model approaches the desired one $r_{\mu_i, \ell \mu_i, \ell}(\tau)$ if the number of exponential functions tends to infinity, i.e., $\hat{r}_{\mu_i, \ell \mu_i, \ell}(\tau) \rightarrow r_{\mu_i, \ell \mu_i, \ell}(\tau)$ as $N_\ell \rightarrow \infty$. By analogy, the substitution of (19a), (19b), and (20) into (18d) and (18e) results for $N_\ell \rightarrow \infty$ and $M_\ell \rightarrow \infty$ in $\hat{r}_{\mu_i, \ell \mu_i^\dagger}(\tau, \chi) \rightarrow r_{\mu_i, \ell \mu_i^\dagger}(\tau, \chi)$ and $\hat{r}_{\mu_1, \ell \mu_2^\dagger}(\tau, \chi) \rightarrow r_{\mu_1, \ell \mu_2^\dagger}(\tau, \chi)$, respectively. For brevity of presentation, only the proof of $\hat{r}_{\mu_1, \ell \mu_2^\dagger}(\tau, \chi) \rightarrow r_{\mu_1, \ell \mu_2^\dagger}(\tau, \chi)$ for $N_\ell \rightarrow \infty$ and $M_\ell \rightarrow \infty$ is shown in Appendix C. Other proofs are omitted here.

Next, the discrete six-tap COST 207 TU channel model [34] with $\alpha = 1 \mu\text{s}$ and $\tau'_{\max} = 7 \mu\text{s}$ will be applied to investigate the degradation effects of the simulation model with a practical limited number of exponential functions. The discrete propagation delays τ'_ℓ of the reference model and the simulation model are then directly equated with the values specified in [34]: $\{\tau'_\ell\}_{\ell=0}^5 = \{0, 0.2, 0.5, 1.6, 2.3, 5\} \mu\text{s}$. Note that the sets $\{\tau'_\ell\}_{\ell=0}^{L-1}$ can also be determined by some other computation methods, e.g., in [14] and [37].

In order to provide a guide on how to choose the number of exponential functions, it is necessary to define some appropriate measures for the errors between the approximate correlation functions and the desired ones. Close observations of (18a), (18d), and (18e) tell us that M_ℓ has no influence on $\hat{r}_{\mu_i, \ell \mu_i, \ell}(\tau) = \hat{r}_{\mu_i, \ell \mu_i^\dagger}(\tau, 0)$, while N_ℓ has no influence on $\hat{r}_{\mu_i, \ell \mu_i^\dagger}(0, \chi)$ and $\hat{r}_{\mu_1, \ell \mu_2^\dagger}(0, \chi)$. A deep insight into the performance and complexity of the wideband-channel simulator can be gained by evaluating the following three performance criteria. The first performance criterion is the mean-square error (MSE) ϵ_1 of the ACF $\hat{r}_{\mu_i, \ell \mu_i, \ell}(\tau)$ defined by

$$\epsilon_1 = \frac{1}{\tau_{\max}} \int_0^{\tau_{\max}} [r_{\mu_i, \ell \mu_i, \ell}(\tau) - \hat{r}_{\mu_i, \ell \mu_i, \ell}(\tau)]^2 d\tau\quad (25)$$

where τ_{\max} denotes an appropriate time interval $[0, \tau_{\max}]$ over which the approximation of $r_{\mu_i, \ell \mu_i, \ell}(\tau)$ is of interest. As suggested in the study in [11], the value $\tau_{\max} = N_\ell / (2f_{\max})$ has turned out to be suitable. The relationship between ϵ_1

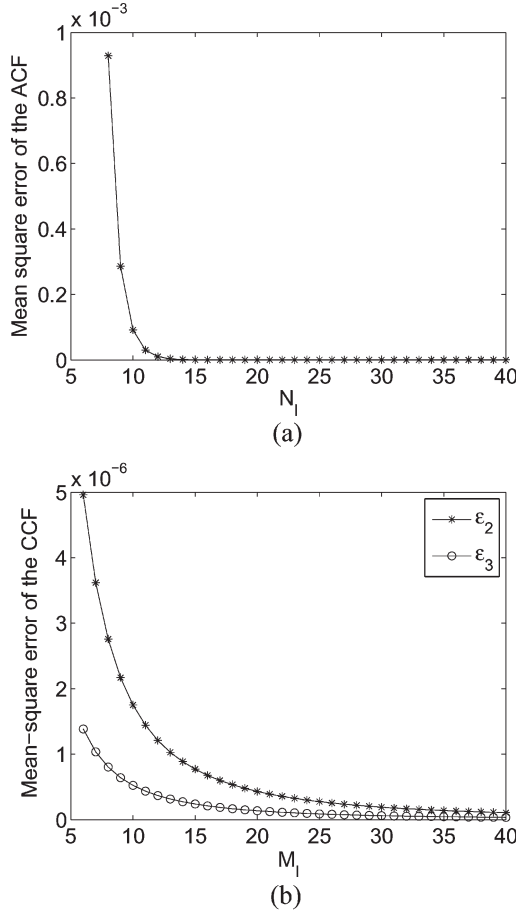


Fig. 3. (a) MSE ϵ_1 of the ACF $\hat{r}_{\mu_i, \ell \mu_i, \ell}(\tau)$ with different N_ℓ . (b) MSEs ϵ_2 of $\hat{r}_{\mu_i, \ell \mu_i, \ell}^\dagger(0, \chi)$ and ϵ_3 of $\hat{r}_{\mu_1, \ell \mu_2, \ell}^\dagger(0, \chi)$ with different M_ℓ for the COST 207 TU channel ($f_{\max} = 91$ Hz, $\alpha = 1$ μ s, $\tau'_{\max} = 7$ μ s), and $\ell = 0$.

and N_ℓ for $\ell = 0$ is given in Fig. 3(a). It clearly illustrates the convergence behavior of $\hat{r}_{\mu_i, \ell \mu_i, \ell}(\tau) \rightarrow r_{\mu_i, \ell \mu_i, \ell}(\tau)$ for increasing N_ℓ . It is apparent that a very good approximation of $\hat{r}_{\mu_i, \ell \mu_i, \ell}(\tau) \approx r_{\mu_i, \ell \mu_i, \ell}(\tau)$ has already been achieved if $N_\ell \geq 15$. The MSEs of the CCFs $\hat{r}_{\mu_i, \ell \mu_i, \ell}^\dagger(0, \chi)$ and $\hat{r}_{\mu_1, \ell \mu_2, \ell}^\dagger(0, \chi)$, which are defined by

$$\epsilon_2 = \frac{1}{\chi_{\max}} \int_0^{\chi_{\max}} \left[r_{\mu_i, \ell \mu_i, \ell}^\dagger(0, \chi) - \hat{r}_{\mu_i, \ell \mu_i, \ell}^\dagger(0, \chi) \right]^2 d\chi \quad (26a)$$

$$\epsilon_3 = \frac{1}{\chi_{\max}} \int_0^{\chi_{\max}} \left[r_{\mu_1, \ell \mu_2, \ell}^\dagger(0, \chi) - \hat{r}_{\mu_1, \ell \mu_2, \ell}^\dagger(0, \chi) \right]^2 d\chi \quad (26b)$$

respectively, are another two important performance criteria. In (26), χ_{\max} represents the maximum frequency separation to which the approximation of $r_{\mu_i, \ell \mu_i, \ell}^\dagger(0, \chi)$ and $r_{\mu_1, \ell \mu_2, \ell}^\dagger(0, \chi)$ is still of interest. Needless to say, χ_{\max} should be larger than or equal to the coherence bandwidth of the channel. It was mentioned in the study in [3] that the coherence bandwidth of a channel in practical cellular systems is on the order of 1–2 MHz. This incites us to choose $\chi_{\max} = 5$ MHz. Both of

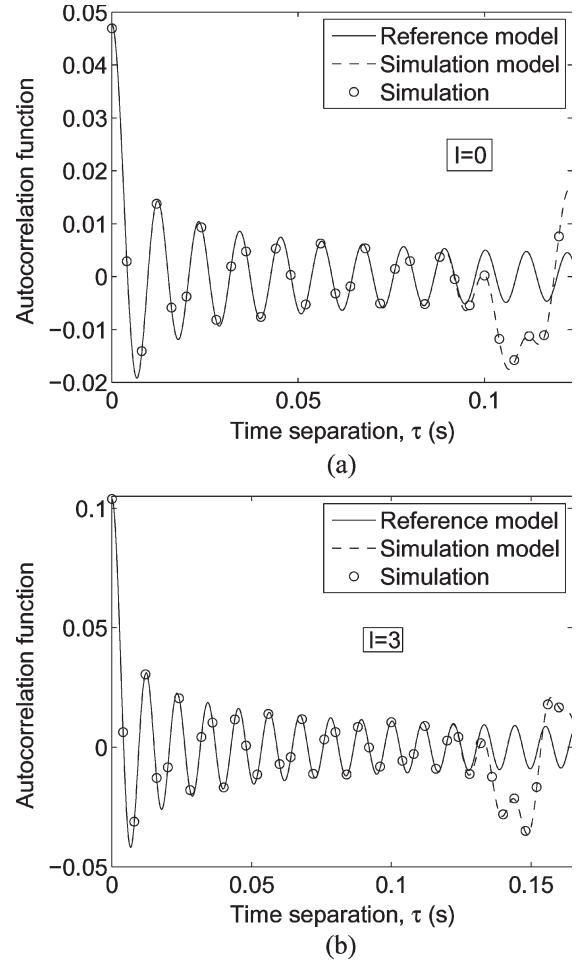


Fig. 4. ACFs $r_{\mu_i, \ell \mu_i, \ell}(\tau)$ of the reference model and $\hat{r}_{\mu_i, \ell \mu_i, \ell}(\tau)$ of the simulation model for the COST 207 TU channel ($f_{\max} = 91$ Hz, $\alpha = 1$ μ s, and $\tau'_{\max} = 7$ μ s). (a) $\ell = 0$, $N_\ell = 15$, and $M_\ell = 20$. (b) $\ell = 3$, $N_\ell = 20$, and $M_\ell = 20$.

the resulting MSEs ϵ_2 and ϵ_3 , in terms of M_ℓ , are shown in Fig. 3(b). This figure demonstrates that ϵ_3 is always smaller than ϵ_2 for the same M_ℓ . However, in both cases, $M_\ell \geq 15$ can always result in very good fittings.

According to the analyses above and taking account of the required condition $N_\ell/N_\lambda \neq (2n-1)/(2k-1)$ for $n = 1, 2, \dots, N_\ell$ and $k = 1, 2, \dots, N_\lambda$, $M_\ell = 20$ ($\ell = 0, 1, \dots, 5$), $N_0 = 15$, $N_1 = 16$, $N_2 = 18$, $N_3 = 20$, $N_4 = 24$, and $N_5 = 32$ were selected for the wideband simulation model as a good compromise between the model's precision and complexity. Fig. 4(a) and (b) impressively shows the excellent accordance between $r_{\mu_i, \ell \mu_i, \ell}(\tau)$ and $\hat{r}_{\mu_i, \ell \mu_i, \ell}(\tau)$ within the time interval $\tau \in [0, N_\ell/(2f_{\max})]$ for $\ell = 0$ and $\ell = 3$, respectively. With the given quantities $f_{\max} = 91$ Hz, $N_0 = 15$, and $N_3 = 20$, $N_0/(2f_{\max}) = 0.0824$ s and $N_3/(2f_{\max}) = 0.1099$ s hold. In case that $\tau > N_\ell/(2f_{\max})$, $\hat{r}_{\mu_i, \ell \mu_i, \ell}(\tau)$ and $r_{\mu_i, \ell \mu_i, \ell}(\tau)$ will gradually diverge and never converge again [11]. In order to check the validity of the analytical expressions, the simulation results obtained by computing the statistical average of 50 random realizations are also illustrated in these figures. To demonstrate the excellent approximation quality of $\hat{r}_{\mu_i, \ell \mu_i, \ell}^\dagger(\tau, \chi) \approx r_{\mu_i, \ell \mu_i, \ell}^\dagger(\tau, \chi)$, the numerical

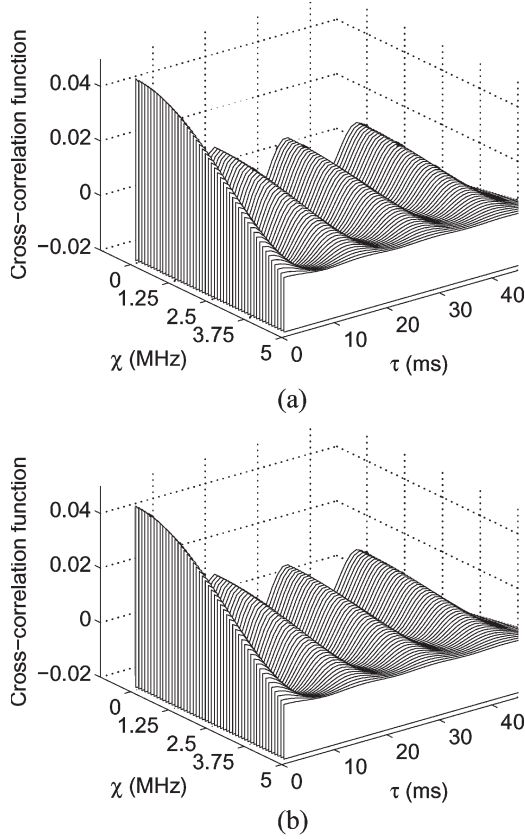


Fig. 5. CCFs for the COST 207 TU channel ($f_{\max} = 91$ Hz, $\alpha = 1$ μ s, and $\tau'_{\max} = 7$ μ s). (a) $r_{\mu_i, \ell \mu_{i, \ell}^\dagger}(\tau, \chi)$ (reference model, $\ell = 0$). (b) $\hat{r}_{\mu_i, \ell \mu_{i, \ell}^\dagger}(\tau, \chi)$ (simulation model, $\ell = 0$, $N_\ell = 15$, and $M_\ell = 20$).

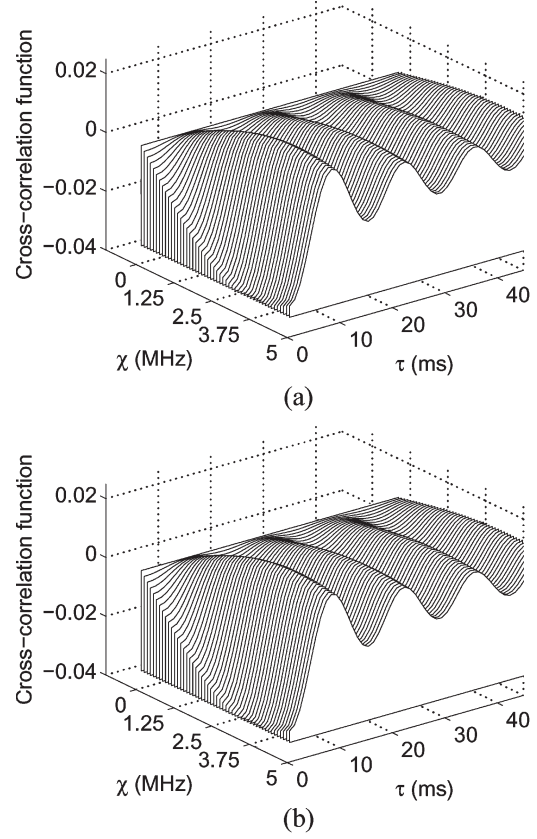


Fig. 6. CCFs for the COST 207 TU channel ($f_{\max} = 91$ Hz, $\alpha = 1$ μ s, and $\tau'_{\max} = 7$ μ s). (a) $r_{\mu_1, \ell \mu_{2, \ell}^\dagger}(\tau, \chi)$ (reference model, $\ell = 0$). (b) $\hat{r}_{\mu_1, \ell \mu_{2, \ell}^\dagger}(\tau, \chi)$ (simulation model, $\ell = 0$, $N_\ell = 15$, and $M_\ell = 20$).

results of (9d) and (18d) for $\ell = 0$ are plotted in Fig. 5(a) and (b), respectively. A good agreement between $r_{\mu_1, \ell \mu_{2, \ell}^\dagger}(\tau, \chi)$ and $\hat{r}_{\mu_1, \ell \mu_{2, \ell}^\dagger}(\tau, \chi)$ is also observed, as shown in Fig. 6 for $\ell = 0$.

B. Comparison of Correlation Functions for Narrowband Rayleigh Fading Channels

The corresponding correlation functions of the narrowband simulation model [see (22a)–(22d)] will be compared with those of the narrowband reference model [see (14a)–(14d)]. Similarly, we can conclude that $\hat{r}_{\mu_1 \mu_2}(\tau) = r_{\mu_1 \mu_2}(\tau) = 0$ always holds. Also, it can easily be shown that $\hat{r}_{\mu_i \mu_i}(\tau) \rightarrow r_{\mu_i \mu_i}(\tau)$, $\hat{r}_{\mu_i \mu_i^\dagger}(\tau, \chi) \rightarrow r_{\mu_i \mu_i^\dagger}(\tau, \chi)$, and $\hat{r}_{\mu_1 \mu_2^\dagger}(\tau, \chi) \rightarrow r_{\mu_1 \mu_2^\dagger}(\tau, \chi)$ as $N \rightarrow \infty$ and $M \rightarrow \infty$.

As a good tradeoff between complexity and performance of the narrowband-channel simulator, $N = 20$ and $M = 20$ were selected. Fig. 7 demonstrates the excellent approximation result for $\hat{r}_{\mu_i \mu_i}(\tau) \approx r_{\mu_i \mu_i}(\tau)$ over the interval $[0, N/(2f_{\max})]$. The simulation result by averaging 50 realizations is also plotted in this figure for the purpose of validation. On the basis of the COST 207 RA channel [34], the numerical results of (14c) and (22c) with the given moderate values of N and M are shown in Fig. 8(a) and (b), respectively. It is clear that $\hat{r}_{\mu_i \mu_i^\dagger}(\tau, \chi)$ matches $r_{\mu_i \mu_i^\dagger}(\tau, \chi)$ very closely.

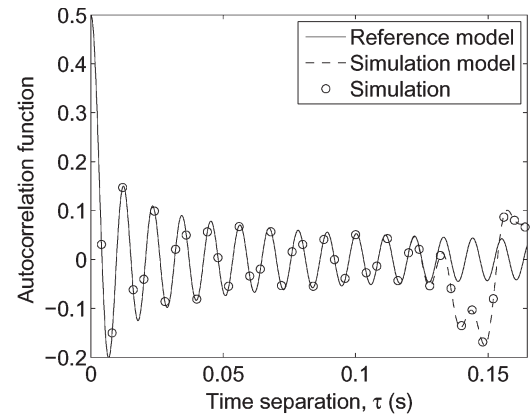


Fig. 7. ACFs $r_{\mu_i \mu_i}(\tau)$ of the reference model and $\hat{r}_{\mu_i \mu_i}(\tau)$ of the simulation model with $N = 20$ and $M = 20$ for $f_{\max} = 91$ Hz.

Fig. 9(a) and (b) indicates that the approximation error between $r_{\mu_1 \mu_2^\dagger}(\tau, \chi)$ and $\hat{r}_{\mu_1 \mu_2^\dagger}(\tau, \chi)$ with the chosen values of N and M is small.

Compared with the two deterministic sum-of-sinusoids channel simulators developed in [25] and [26], the proposed stochastic narrowband Rayleigh fading channel simulator enables better fittings to the underlying reference model, while it has to pay higher computational efforts due to the stochastic property and the used double sum of exponential functions. It should

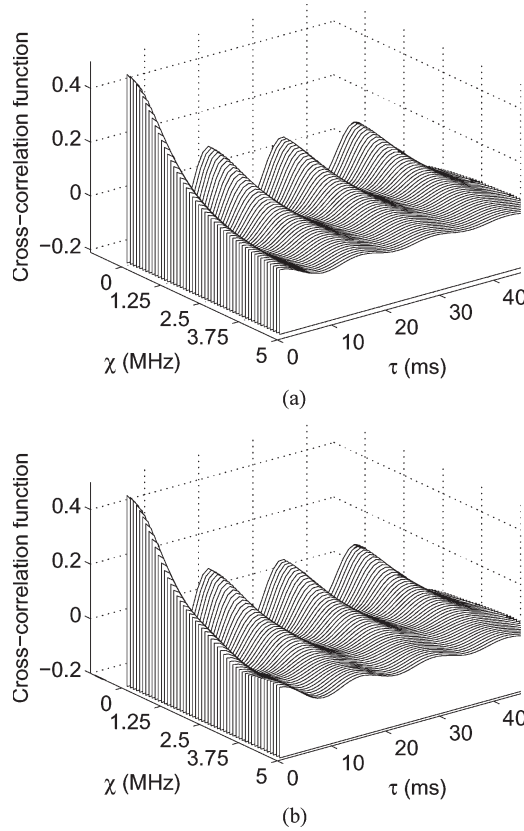


Fig. 8. CCFs for the COST 207 RA channel ($f_{\max} = 91$ Hz and $\alpha = 0.1086 \mu\text{s}$). (a) $r_{\mu_i \mu_i^\dagger}(\tau, \chi)$ of the reference model. (b) $\hat{r}_{\mu_i \mu_i^\dagger}(\tau, \chi)$ of the simulation model with $N = 20$ and $M = 20$.

also be stressed here that this stochastic narrowband-channel simulator has the similar computational complexity to that of the stochastic sum-of-sinusoids channel simulators in [21], [31], and [38]; however, it has the additional capability of directly simulating multiple frequency-correlated Rayleigh fading processes with given temporal and frequency correlation properties.

V. CONCLUSION

In this paper, we have proposed a novel stochastic WSS sum-of-sinusoids channel simulator, which is capable of simulating multiple frequency-correlated wideband and narrowband Rayleigh fading channels. Analytical expressions have been derived for all the parameters of the simulation model. The performance of the proposed channel simulator has been investigated with respect to the ACFs and CCFs of the simulated processes. Three performance criteria have been employed in order to provide a guide on how to choose the number of exponential functions in the channel simulator. The numerical and simulation results show that the correlation properties of the simulation model with the chosen numbers of exponential functions match very closely those of the underlying reference model. The resulting stochastic channel simulator is very useful for the simulation of practical frequency-diversity fading channels, such as FH, MC-CDMA, and OFDM channels.

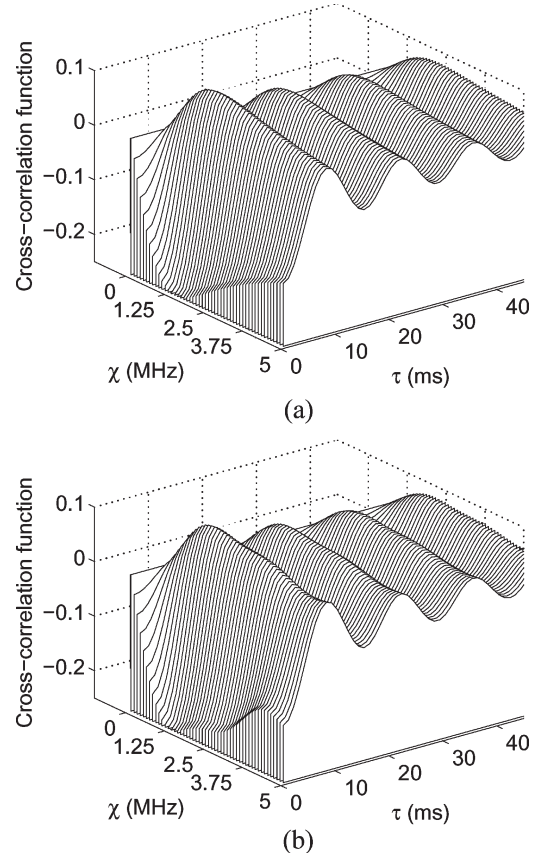


Fig. 9. CCFs for the COST 207 RA channel ($f_{\max} = 91$ Hz, and $\alpha = 0.1086 \mu\text{s}$). (a) $r_{\mu_1 \mu_2^\dagger}(\tau, \chi)$ of the reference model. (b) $\hat{r}_{\mu_1 \mu_2^\dagger}(\tau, \chi)$ of the simulation model with $N = 20$ and $M = 20$.

APPENDIX

A. Derivation of (9e)

In this Appendix, we derive the CCF $r_{\mu_1, \mu_2^\dagger}(\tau, \chi)$ of $\mu_{1, \ell}(t)$ and $\mu_{2, \ell}^\dagger(t)$ according to (8b):

$$\begin{aligned}
 r_{\mu_1, \mu_2^\dagger}(\tau, \chi) &= E \left\{ \mu_{1, \ell}(t) \mu_{2, \ell}^\dagger(t + \tau) \right\} \\
 &= \lim_{\substack{N_\ell \rightarrow \infty \\ M_\ell \rightarrow \infty}} \sum_{n=1}^{N_\ell} \sum_{m=1}^{M_\ell} \sum_{p=1}^{N_\ell} \sum_{q=1}^{M_\ell} \\
 &\quad \times E \left\{ C_{n, m, \ell} C_{p, q, \ell} \right. \\
 &\quad \cdot \cos(2\pi f_{\max} t \cos \beta_{n, \ell}) \\
 &\quad \quad \left. - 2\pi f_c \varphi_{n, m, \ell} - \hat{\theta}_{n, m, \ell} \right\} \\
 &\quad \cdot \sin \left[2\pi f_{\max} (t + \tau) \cos \beta_{p, \ell} \right. \\
 &\quad \quad \left. - 2\pi f_c^\dagger \varphi_{p, q, \ell} - \hat{\theta}_{p, q, \ell} \right] \Big\} \\
 &= \lim_{\substack{N_\ell \rightarrow \infty \\ M_\ell \rightarrow \infty}} \frac{1}{2} \sum_{n=1}^{N_\ell} \sum_{m=1}^{M_\ell} C_{n, m, \ell}^2 \\
 &\quad \times \sin(2\pi f_{\max} \tau \cos \beta_{n, \ell} - 2\pi \chi \varphi_{n, m, \ell}) \\
 &= \lim_{\substack{N_\ell \rightarrow \infty \\ M_\ell \rightarrow \infty}} \frac{1}{2} \sum_{n=1}^{N_\ell} \sum_{m=1}^{M_\ell} p(\beta_{n, \ell}, \varphi_{n, m, \ell}) \\
 &\quad \times \sin(2\pi f_{\max} \tau \cos \beta_{n, \ell} - 2\pi \chi \varphi_{n, m, \ell}) d\beta d\varphi
 \end{aligned}$$

$$\begin{aligned}
&= \frac{1}{2} \int_{\tau'_\ell - \Delta\tau'_\ell/2}^{\tau'_\ell + \Delta\tau'_{\ell+1}/2} \int_0^{2\pi} p(\beta, \varphi) \\
&\quad \times \sin(2\pi f_{\max} \tau \cos \beta - 2\pi \chi \varphi) d\beta d\varphi \\
&= -\frac{1}{2} \int_{\tau'_\ell - \Delta\tau'_\ell/2}^{\tau'_\ell + \Delta\tau'_{\ell+1}/2} \int_0^{2\pi} \frac{1}{2\pi} \frac{b}{\alpha} \exp\left(-\frac{\varphi}{\alpha}\right) \\
&\quad \times \cos(2\pi f_{\max} \tau \cos \beta) \cdot \sin(2\pi \chi \varphi) d\beta d\varphi \\
&= -\frac{bJ_0(2\pi f_{\max} \tau)}{2\alpha} \\
&\quad \times \int_{\tau'_\ell - \Delta\tau'_\ell/2}^{\tau'_\ell + \Delta\tau'_{\ell+1}/2} \exp\left(-\frac{\varphi}{\alpha}\right) \sin(2\pi \chi \varphi) d\varphi. \quad (27)
\end{aligned}$$

The indefinite integral in the right-hand side of the above equation can be solved by using [39, eq. (2.663.1)] as follows:

$$\begin{aligned}
&\int \exp\left(-\frac{\varphi}{\alpha}\right) \sin(2\pi \chi \varphi) d\varphi \\
&= \frac{\exp\left(-\frac{\varphi}{\alpha}\right) \left[-\frac{1}{\alpha} \sin(2\pi \chi \varphi) - 2\pi \chi \cos(2\pi \chi \varphi)\right]}{\frac{1}{\alpha^2} + (2\pi \chi)^2} \\
&= \frac{-\alpha \exp\left(-\frac{\varphi}{\alpha}\right)}{1 + (2\pi \alpha \chi)^2} [\sin(2\pi \chi \varphi) + 2\pi \alpha \chi \cos(2\pi \chi \varphi)]. \quad (28)
\end{aligned}$$

The substitution of (28) to (27) leads to an expression of $r_{\mu_{1,\ell}\mu_{2,\ell}^\dagger}(\tau, \chi)$ shown in (9e).

B. Derivation of (20)

In this Appendix, we apply the parameter-computation method proposed in the study in [23] to derive a closed-form expression for the discrete delays $\phi_{m,\ell}$ shown in (20). Close observations of the expressions (18a)–(18f) show us that the discrete delays $\phi_{m,\ell}$ appear only in (18d) and (18e). Therefore, we will calculate $\phi_{m,\ell}$ in such a way that for a limited number of exponential functions, $\hat{r}_{\mu_{i,\ell}\mu_{i,\ell}^\dagger}(0, \chi)$ and $\hat{r}_{\mu_{1,\ell}\mu_{2,\ell}^\dagger}(0, \chi)$ can approximate as well as possible $r_{\mu_{i,\ell}\mu_{i,\ell}^\dagger}(0, \chi)$ and $r_{\mu_{1,\ell}\mu_{2,\ell}^\dagger}(0, \chi)$, respectively.

Beginning with the first pair $\hat{r}_{\mu_{i,\ell}\mu_{i,\ell}^\dagger}(0, \chi)$ and $r_{\mu_{i,\ell}\mu_{i,\ell}^\dagger}(0, \chi)$, we obtain their Fourier transforms as follows:

$$\begin{aligned}
\hat{S}_{\mu_{i,\ell}\mu_{i,\ell}^\dagger}(\phi) &= \frac{b}{4M_\ell} (A_\ell - B_\ell) \\
&\quad \cdot \sum_{m=1}^{M_\ell} [\delta(\phi - \phi_{m,\ell}) + \delta(\phi + \phi_{m,\ell})] \quad (29a)
\end{aligned}$$

$$S_{\mu_{i,\ell}\mu_{i,\ell}^\dagger}(\phi) = \frac{b}{4\alpha} \exp\left(-\frac{\phi}{\alpha}\right). \quad (29b)$$

By comparing (29b) with (7), it is clear that $S_{\mu_{i,\ell}\mu_{i,\ell}^\dagger}(\phi)$ is related to the PDP, as is $\hat{S}_{\mu_{i,\ell}\mu_{i,\ell}^\dagger}(\phi)$. Let us introduce the intervals $I_m = (\phi_{m-1,\ell}, \phi_{m,\ell}]$ with $\phi_{0,\ell} = \tau'_\ell - \Delta\tau'_\ell/2$. We demand that

the average delay power of the reference model is equal to the average delay power of the simulation model within the interval I_m , i.e.,

$$\int_{\phi \in I_m} S_{\mu_{i,\ell}\mu_{i,\ell}^\dagger}(\phi) d\phi = \int_{\phi \in I_m} \hat{S}_{\mu_{i,\ell}\mu_{i,\ell}^\dagger}(\phi) d\phi \quad (30)$$

for $m = 1, 2, \dots, M_\ell$. To solve this problem, we define an auxiliary function according to

$$G(\phi_{m,\ell}) := \int_0^{\phi_{m,\ell}} S_{\mu_{i,\ell}\mu_{i,\ell}^\dagger}(\phi) d\phi. \quad (31)$$

Applying (29b), we can write

$$G(\phi_{m,\ell}) = \frac{b}{4} \left[1 - \exp\left(-\frac{\phi_{m,\ell}}{\alpha}\right) \right]. \quad (32)$$

If we keep (30) in mind and use (29a) and (31), another form of $G(\phi_{m,\ell})$ can be obtained:

$$\begin{aligned}
G(\phi_{m,\ell}) &= \int_0^{\tau'_\ell - \Delta\tau'_\ell/2} S_{\mu_{i,\ell}\mu_{i,\ell}^\dagger}(\phi) d\phi + \sum_{k=1}^m \int_{\phi \in I_k} S_{\mu_{i,\ell}\mu_{i,\ell}^\dagger}(\phi) d\phi \\
&= \frac{b}{4} (1 - A_\ell) + \sum_{k=1}^m \int_{\phi \in I_k} \hat{S}_{\mu_{i,\ell}\mu_{i,\ell}^\dagger}(\phi) d\phi \\
&= \frac{b}{4} (1 - A_\ell) + \frac{bm}{4M_\ell} (A_\ell - B_\ell). \quad (33)
\end{aligned}$$

The comparison between (32) and (33) leads to an analytical expression for the discrete delays $\phi_{m,\ell}$, as given in (20). Applying the above proposed computation procedure, the same result for $\phi_{m,\ell}$ can be achieved from another relation pair $\hat{r}_{\mu_{1,\ell}\mu_{2,\ell}^\dagger}(0, \chi)$ and $r_{\mu_{1,\ell}\mu_{2,\ell}^\dagger}(0, \chi)$.

C. Proof of $\hat{r}_{\mu_{1,\ell}\mu_{2,\ell}^\dagger}(\tau, \chi) \rightarrow r_{\mu_{1,\ell}\mu_{2,\ell}^\dagger}(\tau, \chi)$ for $N_\ell \rightarrow \infty$ and $M_\ell \rightarrow \infty$

Performing the substitution of (19a) and (19b) and (20) into (18e) gives, for $N_\ell \rightarrow \infty$, and $M_\ell \rightarrow \infty$, the following desired result:

$$\begin{aligned}
&\lim_{\substack{N_\ell \rightarrow \infty \\ M_\ell \rightarrow \infty}} \hat{r}_{\mu_{1,\ell}\mu_{2,\ell}^\dagger}(\tau, \chi) \\
&= \lim_{\substack{N_\ell \rightarrow \infty \\ M_\ell \rightarrow \infty}} \sum_{n=-N_\ell+1}^{N_\ell} \sum_{m=1}^{M_\ell} \frac{b(A_\ell - B_\ell)}{4N_\ell M_\ell} \\
&\quad \cdot \sin \left\{ 2\pi f_{\max} \tau \cdot \sin \left[\frac{\pi}{2N_\ell} \left(n - \frac{1}{2} \right) \right] \right. \\
&\quad \left. - 2\pi \alpha \chi \ln \left[\frac{1}{A_\ell - \frac{m}{M_\ell} (A_\ell - B_\ell)} \right] \right\}
\end{aligned}$$

$$\begin{aligned}
&= \lim_{N_\ell \rightarrow \infty} \sum_{n=-N_\ell+1}^{N_\ell} \frac{b(A_\ell - B_\ell)}{4N_\ell} \\
&\quad \times \int_0^1 \sin \left\{ 2\pi f_{\max} \tau \cdot \sin \left[\frac{\pi}{2N_\ell} \left(n - \frac{1}{2} \right) \right] \right. \\
&\quad \quad \left. - 2\pi\alpha\chi \ln \left[\frac{1}{A_\ell - x(A_\ell - B_\ell)} \right] \right\} dx \\
&= \lim_{N_\ell \rightarrow \infty} \sum_{n=-N_\ell+1}^{N_\ell} \frac{b}{4N_\ell} \int_{\alpha \ln(\frac{1}{A_\ell})}^{\alpha \ln(\frac{1}{B_\ell})} \frac{1}{\alpha} \exp\left(-\frac{z}{\alpha}\right) \\
&\quad \cdot \sin \left\{ 2\pi f_{\max} \tau \sin \left[\frac{\pi}{2N_\ell} \left(n - \frac{1}{2} \right) \right] - 2\pi\chi z \right\} dz \\
&= \frac{b}{2\pi} \int_{-\frac{\pi}{2}}^{\frac{\pi}{2}} \int_{\alpha \ln(\frac{1}{A_\ell})}^{\alpha \ln(\frac{1}{B_\ell})} \frac{1}{\alpha} \exp\left(-\frac{z}{\alpha}\right) \\
&\quad \cdot \sin(2\pi f_{\max} \tau \sin y - 2\pi\chi z) dz dy \\
&= -\frac{b}{2\pi\alpha} \int_{-\frac{\pi}{2}}^{\frac{\pi}{2}} \cos(2\pi f_{\max} \tau \sin y) dy \\
&\quad \cdot \int_{\alpha \ln(\frac{1}{A_\ell})}^{\alpha \ln(\frac{1}{B_\ell})} \exp\left(-\frac{z}{\alpha}\right) \sin(2\pi\chi z) dz \\
&= \frac{bJ_0(2\pi f_{\max} \tau)}{2[1 + (2\pi\alpha\chi)^2]} \exp\left(-\frac{z}{\alpha}\right) \\
&\quad \cdot [\sin(2\pi\chi z) + 2\pi\alpha\chi \cos(2\pi\chi z)] \Big|_{z=\tau'_\ell - \Delta\tau'_\ell/2}^{z=\tau'_\ell + \Delta\tau'_\ell/2} \\
&= r_{\mu_{1,\ell}\mu_{2,\ell}^\dagger}(\tau, \chi). \tag{34}
\end{aligned}$$

Thus, $\hat{r}_{\mu_{1,\ell}\mu_{2,\ell}^\dagger}(\tau, \chi)$ converges to $r_{\mu_{1,\ell}\mu_{2,\ell}^\dagger}(\tau, \chi)$ if $N_\ell \rightarrow \infty$ and $M_\ell \rightarrow \infty$.

ACKNOWLEDGMENT

The authors would like to thank the anonymous reviewers for their helpful and constructive comments.

REFERENCES

- [1] W. C. Jakes, Ed., *Microwave Mobile Communications*. Piscataway, NJ: IEEE Press, 1994.
- [2] T. C. Wu, C. C. Chao, and K. C. Chen, "Capacity of synchronous coded DS SFH and FFH spread-spectrum multiple-access for wireless local communications," *IEEE Trans. Commun.*, vol. 45, no. 2, pp. 200–212, Feb. 1997.
- [3] Z. Kotic, I. Maric, and X. D. Wang, "Fundamentals of dynamic FH in cellular systems," *IEEE J. Sel. Areas Commun.*, vol. 19, no. 11, pp. 2254–2266, Nov. 2001.
- [4] N. C. Beaulieu, "Generation of correlated Rayleigh fading envelopes," *IEEE Commun. Lett.*, vol. 3, no. 6, pp. 172–174, Jun. 1999.
- [5] B. Natarajan, C. R. Nassar, and V. Chandrasekhar, "Generation of correlated Rayleigh fading envelopes for spread spectrum applications," *IEEE Commun. Lett.*, vol. 4, no. 1, pp. 9–11, Jan. 2000.
- [6] S. Sorooshyari and D. G. Daut, "Generation of correlated Rayleigh fading envelopes for accurate performance analysis of diversity systems," in *Proc. IEEE PIMRC*, Beijing, China, Sep. 2003, pp. 1800–1804.
- [7] T. Kligenbrunn and P. Mogensen, "Modeling frequency correlation of fast fading in frequency hopping GSM link simulations," in *Proc. IEEE VTC—Fall*, Amsterdam, The Netherlands, Sep. 1999, pp. 2398–2402.
- [8] N. C. Beaulieu and M. L. Merani, "Efficient simulation of correlated diversity channels," in *Proc. IEEE WCNC*, Chicago, IL, Sep. 2000, pp. 207–210.
- [9] S. O. Rice, "Mathematical analysis of random noise," *Bell Syst. Tech. J.*, vol. 23, pp. 282–332, Jul. 1944.
- [10] S. O. Rice, "Mathematical analysis of random noise," *Bell Syst. Tech. J.*, vol. 24, pp. 46–156, Jan. 1945.
- [11] M. Pätzold, *Mobile Fading Channels*. New York: Wiley, 2002.
- [12] P. Höher, "A statistical discrete-time model for the WSSUS multipath channel," *IEEE Trans. Veh. Technol.*, vol. 41, no. 4, pp. 461–468, Nov. 1992.
- [13] K. W. Yip and T. S. Ng, "Karhunen-Loève expansion of the WSSUS channel output and its application to efficient simulation," *IEEE J. Sel. Areas Commun.*, vol. 15, no. 4, pp. 640–646, May 1997.
- [14] E. Chiavaccini and G. M. Vitetta, "GQR models for multipath Rayleigh fading channels," *IEEE J. Sel. Areas Commun.*, vol. 19, no. 6, pp. 1009–1018, Jun. 2001.
- [15] M. Pätzold and N. Youssef, "Modeling and simulation of direction-selective and frequency-selective mobile radio channels," *Int. J. Electr. Commun.*, vol. AEÜ-55, no. 6, pp. 433–442, Nov. 2001.
- [16] Q. Yao and M. Pätzold, "Down-link channel modeling for mobile communications with smart antennas at the base station," in *Proc. IEEE VTC—Spring*, Jeju, Korea, Apr. 2003, pp. 321–325.
- [17] C. X. Wang and M. Pätzold, "A generative deterministic model for digital mobile fading channels," *IEEE Commun. Lett.*, vol. 8, no. 4, pp. 223–225, Apr. 2004.
- [18] C. X. Wang and M. Pätzold, "A new deterministic process based generative model for characterizing bursty error sequences," in *Proc. IEEE PIMRC*, Barcelona, Spain, Sep. 2004, pp. 2134–2139.
- [19] P. Dent, G. E. Bottomley, and T. Croft, "Jakes fading model revisited," *Electron. Lett.*, vol. 29, no. 13, pp. 1162–1163, Jun. 1993.
- [20] Y. B. Li and Y. L. Guan, "Modified Jakes model for simulating multiple uncorrelated fading waveforms," in *Proc. IEEE ICC*, New Orleans, LA, Jun. 2000, pp. 46–49.
- [21] Y. R. Zheng and C. Xiao, "Improved models for the generation of multiple uncorrelated Rayleigh fading waveforms," *IEEE Commun. Lett.*, vol. 6, no. 6, pp. 256–258, Jun. 2002.
- [22] Y. Li and X. Huang, "The simulation of independent Rayleigh faders," *IEEE Trans. Commun.*, vol. 50, no. 9, pp. 1503–1514, Sep. 2002.
- [23] C. X. Wang and M. Pätzold, "Methods of generating multiple uncorrelated Rayleigh fading processes," in *Proc. IEEE VTC—Spring*, Jeju, Korea, Apr. 2003, pp. 510–514.
- [24] C. X. Wang and M. Pätzold, "Efficient simulation of multiple cross-correlated Rayleigh fading channels," in *Proc. IEEE PIMRC*, Beijing, China, Sep. 2003, pp. 1526–1530.
- [25] M. Pätzold, F. Laue, and U. Killat, "A frequency hopping Rayleigh fading channel simulator with given correlation properties," in *Proc. IEEE ISPACS*, Kuala Lumpur, Malaysia, Nov. 1997, pp. S8.1.1–S8.1.6.
- [26] C. X. Wang, M. Pätzold, and B. Itsarachai, "A deterministic frequency hopping Rayleigh fading channel simulator designed by using optimization techniques," in *Proc. IEEE PIMRC*, Lisbon, Portugal, Sep. 2002, pp. 478–483.
- [27] J. D. Parsons, *The Mobile Radio Propagation Channel*, 2nd ed. New York: Wiley, 2000.
- [28] G. L. Stüber, *Principles of Mobile Communications*, 2nd ed. Boston, MA: Kluwer, 2001.
- [29] R. H. Clarke, "A statistical theory of mobile-radio reception," *Bell Syst. Tech. J.*, vol. 47, no. 6, pp. 957–1000, Jul./Aug. 1968.
- [30] M. F. Pop and N. C. Beaulieu, "Limitations of sum-of-sinusoids fading channel simulators," *IEEE Trans. Commun.*, vol. 49, no. 4, pp. 699–708, Apr. 2001.
- [31] M. F. Pop and N. C. Beaulieu, "Design of wide-sense stationary sum-of-sinusoids fading channel simulators," in *Proc. IEEE ICC*, New York, Apr. 28–May 2 2002, pp. 709–716.
- [32] M. Pätzold, "On the stationarity and ergodicity of fading channel simulators basing on Rice's sum-of-sinusoids," in *Proc. IEEE PIMRC*, Beijing, China, Sep. 2003, pp. 1526–1530.

- [33] P. A. Bello, "Characterization of randomly time-variant linear channels," *IEEE Trans. Commun.*, vol. COM-11, no. 4, pp. 360–393, Dec. 1963.
- [34] "Digital land mobile radio communications," *Office for Official Publications of the European Communities*, 1989, Luxembourg. Final Report.
- [35] J. C. Silva, N. Souto, A. Rodrigues, F. Cercas, and A. Correia, "Conversion of reference tapped delay line channel models to discrete time channel models," in *Proc. IEEE VTC—Fall*, Orlando, FL, Oct. 2003, pp. 128–132.
- [36] A. Papoulis and S. U. Pillai, *Probability, Random Variables and Stochastic Processes*, 4th ed. New York: McGraw-Hill, 2002.
- [37] M. Pätzold, A. Szczepanski, and N. Youssef, "Methods for modeling of specified and measured multipath power-delay profiles," *IEEE Trans. Veh. Technol.*, vol. 51, no. 5, pp. 978–988, Sep. 2002.
- [38] C. Xiao, Y. R. Zheng, and N. C. Beaulieu, "Second-order statistical properties of the WSS Jakes' fading channel simulator," *IEEE Trans. Commun.*, vol. 50, no. 6, pp. 888–891, Jun. 2002.
- [39] I. S. Gradshteyn and I. M. Ryzhik, *Tables of Integrals, Series, and Products*, 6th ed. Boston, MA: Academic, 2000.



Cheng-Xiang Wang (S'01–M'05) received the B.Sc. and M.Eng. degrees in communication and information systems from Shandong University, Shandong, China, in 1997 and 2000, respectively, and the Ph.D. degree in wireless communications from Aalborg University, Aalborg, Denmark, in 2004.

From 2000 to 2001, he was a Research Assistant with the Department of Communication Networks, Technical University of Hamburg–Harburg, Hamburg, Germany. From 2001 to 2005, he was a Research Fellow of mobile communications with Agder University College, Grimstad, Norway. From January to April 2004, he was a Visiting Researcher at the Baseband Algorithms and Standardization Laboratory, Siemens AG-Mobile Phones, Munich, Germany, conducting research and development of error models for Enhanced General Packet Radio Service (EGPRS) systems within the framework of the 3GPP GERAN System Concept R&D Project. Since 2005, he has been a Lecturer in Mobile Communications and Networks at Heriot–Watt University, Edinburgh, U.K. He is also an honorary fellow of the University of Edinburgh and has been an Adjunct Professor with Guilin University of Electronic Technology, Guilin, China, since June 2006. His current research interests include mobile propagation channel modeling, error models, smart antennas and (virtual) multiple-input–multiple-output systems, orthogonal frequency-division multiplexing, ultrawideband, cognitive radio, space-time coding, cross-layer design of wireless networks, mobile *ad hoc* and wireless-sensor networks, and 3GPP long-term evolution. He has published about 70 research papers in journals and conference proceedings.

Dr. Wang was the recipient of the "1999 Excellent Paper Award" for two of his papers from the Sixth National Youth Communication Conference of China, Beijing, China. He serves as an Editorial Board Member of the *Wireless Communications and Mobile Computing* (WCMC) and as a Technical Program Committee Member for 14 major international conferences, including IEEE VTC 2005–Fall, ICIC 2006, Globecom 2006, WCNC 2007, ICC 2007, and ICIC 2007. He also served as Session Chair for ICCAS 2006. He is a member of the Institute of Engineering and Technology (IET).



Matthias Pätzold (M'94–SM'98) received the Dipl.-Ing. and Dr.-Ing. degrees in electrical engineering from Ruhr-University Bochum, Bochum, Germany, in 1985 and 1989, respectively, and the Habilitation degree in communications engineering from the Technical University of Hamburg–Harburg, Hamburg, Germany, in 1998.

From 1990 to 1992, he was with ANT Nachrichtentechnik GmbH, Backnang, Germany, where he was engaged in digital satellite communications.

From 1992 to 2001, he was with the Department of Digital Networks at the Technical University Hamburg–Harburg. Since 2001, he has been a Full Professor of mobile communications with Agder University College, Grimstad, Norway. He is the Author of the books *Mobile Radio Channels—Modelling, Analysis, and Simulation* (in German) (Vieweg, 1999) and *Mobile Fading Channels* (Wiley & Sons, 2002). His current research interests include mobile-radio communications, particularly multipath fading-channel modeling, multiple-input–multiple-output systems, channel-parameter estimation, and coded-modulation techniques for fading channels.

Prof. Pätzold was the recipient of the "1998 and 2002 Neal Shepherd Memorial Best Propagation Paper Award" from the IEEE Vehicular Technology Society. He was the recipient of the "2003 Excellent Paper Award" from the IEEE International Symposium on Personal, Indoor, and Mobile Radio Communications (PIMRC'03) in Beijing, China, as well as of the "Best Paper Award" from the eighth International Symposium on Wireless Personal Multimedia Communications (WPMC'05) in Aalborg, Denmark. He was Local Organizer of the conference "Kommunikation in Verteilten Systemen (KiVS) 2001" and Organizer of the second International Workshop on "Research Directions in Mobile Communications and Services 2002." He served as a member of the Technical Program Committee for IST'05, VTC'05–Fall, and WPMC'05. He also served as Session Chair for several reputed international conferences (VTC'04–Spring, NRS'04, PIMRC'04, IST'05, and WPMC'05).



Qi Yao received the B.Sc. and M.Eng. degrees in communication and information systems from Shandong University, Shandong, China, in 1997 and 2000, respectively. She is currently working toward the Ph.D. degree at Aalborg University, Aalborg, Denmark.

In 2001, she worked as a Student Research Assistant with the Department of Communication Networks, Technical University Hamburg–Harburg, Hamburg, Germany. Since October 2001, she has been with Agder University College, Grimstad, Norway. Her current research interests include mobile communications, adaptive antenna systems, mobile fading-channel modeling, and channel-parameter estimation.